Principles of Meiotic Chromosome Assembly

*Stephanie A. Schalbetter[1], *Geoffrey Fudenberg[2], Jonathan Baxter[1], Katherine S. Pollard[2,3,4], and Matthew J. Neale[1]

*SAS and GF contributed equally to this work

1. Genome Damage and Stability Centre, School of Life Sciences, University of Sussex, UK
2. Gladstone Institute of Data Science and Biotechnology, San Francisco, USA
3. Department of Epidemiology & Biostatistics, Institute for Human Genetics, Quantitative Biology Institute, and Institute for Computational Health Sciences, University of California, San Francisco, California, USA.
4. Chan-Zuckerberg Biohub, San Francisco, California, USA.

Abstract

During meiotic prophase, chromosomes organise into a series of chromatin loops emanating from a proteinaceous axis. Yet, while much is known about meiotic chromosome morphology, the mechanism of assembly, and how assembly is regulated, remain open questions. Here we combine genome-wide chromosome conformation analysis (Hi-C) with *Saccharomyces cerevisiae* genetics and *in silico* polymer modelling to elucidate the mechanisms that shape meiotic chromosomes. Entering meiosis, grid-like Hi-C interaction patterns emerge that correspond to the localisation of—and depend upon—the meiotic cohesin subunit Rec8. Such patterns fit a model of loop extrusion, where a heterogeneous population of expanding loops develop along the chromosome, with growth limited by barriers. While grid-like patterns emerge independently of chromosome synapsis, synapsis itself generates additional compaction that matures differentially depending on telomeric distance and chromosome size. Our results elucidate fundamental principles of meiotic chromosome assembly and demonstrate the essential role of cohesin within this evolutionarily conserved process.

Introduction and results

During meiosis, eukaryotic chromosomes are broken, repaired and paired with their homologs followed by two rounds of segregation—a series of events accompanied by dynamic structural changes of the chromosomes. Most prominent is the arrangement of pachytene chromosomes into a dense array of chromatin loops emanating from a central proteinaceous core, the synaptonemal complex (SC), which is highly conserved across eukaryotes[1,2]. In *S. cerevisiae*,

SC components include the meiotic cohesin kleisin subunit, Rec8[3], the transverse filament, Zip1[4], the axial/lateral elements, Hop1 and Red1[5,6], and the pro-DSB factors Rec114-Mei4-Mer2 (RMM)[7,8]. Much of our understanding of meiotic chromosome structure has been deduced from a combination of electron microscopy, immunofluorescence microscopy, and the genome-wide patterns of protein localisation determined by ChIP. However, the link between key meiotic protein complexes, chromosome conformation, and genomic sequence remains uncharacterized.

Chromosome conformation capture (3C) techniques generate maps of pairwise contact frequencies that are snapshots of chromosome organisation. 3C methods were originally applied to assay chromosome conformation in *S. cerevisiae*, including during meiosis[9]. Now they are widely used across a range of organisms and cellular contexts to link 3D organisation directly with genomic sequence[10], revealing important roles of the Structural Maintenance of Chromosomes (SMCs) cohesin and condensin in genomic organization[11,12], where they likely mediate chromosome compaction via the process of loop extrusion[13]. Here we return to yeast meiosis to interrogate genome-wide chromosome organisation by Hi-C, elucidate mechanisms of chromosome assembly, and define the role of key meiotic chromosome components, including cohesin and the SC.

Starting with a synchronized G1 population we analysed timepoints encompassing DNA replication, meiotic prophase and both meiotic divisions (**Fig. 1a,b,c, Extended Data Fig. 1a,b,c**). In G1, we detect strong centromere clustering (**Fig. 1a,d**) and folding back of the arms at the centromeres (**Fig. 1a, Supplementary Fig. 2**), characteristic of a Rabl conformation[9,14]. During meiosis, centromere clustering is transiently dissolved (3-5h, **Fig. 1a,d, Extended Data Fig. 1a**); this coincides with a global decrease in inter-chromosomal contact frequency at mid-prophase, reflecting chromosome individualisation. Subtelomeric clustering also decreases during meiotic prophase (**Fig. 1a,d, Extended Data Fig. 1a**), with no evidence for the transient telomeric bouquet conformation, consistent with prior microscopic analyses[15].

Entering meiosis, contact frequency versus distance, *P(s),* curves display a shoulder, consistent with the linear compaction of chromosome arms increasing due to *cis*-loop formation (2-4h, **Fig. 1e, Extended Data Fig. 1d**, e.g. as defined[16]; for review[13]). This change in *P(s)* is reminiscent of the SMC-dependent changes observed via Hi-C during mitosis across species[17–21]. Compaction coincides with meiotic prophase I and the formation of the SC at pachytene, and is lost at later stages (**Fig. 1e, Extended Data Fig. 1d**).

To study meiotic chromosome conformation in more detail, and to eliminate cell-to-cell heterogeneity (**Fig. 1b,c**), we enriched for pachytene cells in subsequent experiments by inactivating Ndt80, a transcription factor required for exit from meiotic prophase[22]. *ndt80*Δ cells enter meiosis synchronously, assessed by bulk DNA replication (**Fig. 1f**), but do not initiate the first nuclear division[22]. Similar to the wild type prophase population (3-5 h), but likely accentuated by the increased homogeneity, Hi-C maps of pachytene-enriched cells displayed total loss of centromere clustering (**Extended Data Fig. 2**) and dramatic chromosome arm compaction (**Fig. 1e**). Analysing compaction in more detail, shorter chromosomes (**Extended Data Fig. 1e**) and, in particular, shorter chromosome arms (**Fig. 1h, Extended Data Fig. 1f**), displayed elevated contact frequency at short genomic separations, and an earlier shoulder, apparently arising from distinct behavior of subtelomeric and subcentromeric regions (**Fig. 1h, Extended Data Fig. 1g**). Moreover, distinct *P(s)* for chromosomes with different length arms (**Extended Data Fig. 1h**) suggests that the centromere can insulate the process that leads to differences between arms. In agreement with this, compaction is interrupted at centromeres in Hi-C maps (**Fig. 1a**, **Extended Data Fig. 2b**).

Zooming in to consider within-arm organisation revealed punctate grid-like Hi-C interactions between pairs of loci during prophase (**Fig. 2a**), particularly prominent in *ndt80*Δ (**Fig. 2a,b**). Such patterns have not been observed in yeast[19,21], human[20,23], or chicken[17] mitotic chromosomes, which all display locus-independent compaction along chromosome arms. The focal meiotic patterns we observe are more prominent than reported previously[24]— resembling peaks between CTCF sites[25] rather than topological domains[26,27] detected in mammalian interphase Hi-C maps—and likely arise from a heterogeneous mixture of 'transitive' interactions and 'skipping' of peak bases (**Fig. 2c**).

Genomic regions underlying the punctate Hi-C interactions display a remarkable visual (**Fig. 2a,b**), and quantitative (**Fig. 2d-g**), correspondence with previously characterised sites of high Rec8 occupancy[28]. At pachytene, Rec8 sites display elevated *cis*/total contact frequencies (**Fig. 2d**), enriched contact frequency (**Fig. 2e,f**), and evidence of insulation (**Fig. 2g**)—features that correlate with Rec8 occupancy measured by ChIP (**Fig. 2a, lower**). In wild type cells, Rec8-Rec8 interactions became visible in early prophase (2 h) peaked at mid prophase (4 h), and were especially prominent in the homogenous *ndt80*Δ cell population (**Fig. 2a-g, Extended Data Fig. 4b,c**). Importantly, Rec8-Rec8 enrichments are strongest between adjacent sites, decrease between non-adjacent sites with increasing genomic separation, and are absent in *trans* (**Extended Data Fig. 4b,c**). As for enrichments between CTCF sites in mammalian

interphase[29], these observations argue that a cis-acting process generates such focal interactions in meiosis.

Rec8 is a central component of the meiotic chromosome axis[3]. Assaying a *rec8*Δ mutant enabled us to determine that Rec8 is absolutely required for the emergence of the grid-like Hi-C patterns present in meiosis (**Fig. 2a,b**). Moreover, *rec8*Δ cells completely lose the shoulder in *P(s)*, indicative of a dramatic loss of arm compaction (**Fig. 2b, Extended Data Fig. 4a**), similar to that caused by depletion of SMCs in diverse contexts[17,19,21,30–32]. Instead of assembling an axis of loops, *rec8*Δ cells appear to be caught in a state with highly clustered telomeres (**Extended Data Fig. 4d, Extended Data Fig. 3**), consistent with previous observations by microscopy[33,34]. Moreover, in *rec8*Δ cells *cis* contact frequency is reduced (**Fig. 2d**), similar to G1 cells, and cis/total no longer correlates with Rec8 occupancy. Instead, *rec8*Δ cis/total displays a decreasing trend along chromosome arms, likely due to persistent telomere clustering (**Extended Data Fig. 4d**).

To test how compaction and grid-like interaction patterns could jointly emerge in meiosis, we developed polymer simulations (**Fig. 3a, Methods**) similar to those used to successfully describe the assembly of TADs in mammalian interphase chromosomes[13]. Importantly, these simulations employ the *cis*-acting process of loop extrusion, where extruders dynamically form progressively larger chromatin loops, unless impeded by adjacent extruders or barrier elements (**Fig. 3a**). Because the accumulation of Rec8 at ChIP-seq sites[28] concomitant with convergent transcription[35] is indicative of barriers to extrusion[29], we positioned bi-directional barriers at Rec8 sites.

Simulations were used to explore variations in loop extrusion dynamics to determine whether specific parameter combinations are able to generate Hi-C maps that agree with experimental observation (**Fig. 3, Methods**). Models with excellent fits were identified in which ~65% of the genome is covered by extruded loops (**Fig. 3b,c, Extended Data Fig. 5**)—a far denser array than present in *S. cerevisiae* mitosis[21], but still less compact than human mitotic cells[20]. Even though extrusion can generate compaction independently of barriers (**Fig. 3d**), an intermediate barrier strength is essential to match the grid-like patterns observed experimentally (**Fig. 3b**). Despite the simplifying assumptions, simulated chromosomes displayed many features observed experimentally: (i) chromosomes fold into a loose polymer brush[3,36,37], with a Rec8-rich core[3] (**Fig. 3f, Extended Data Fig. 5a**); (ii) a grid-like interaction pattern naturally emerges in simulated Hi-C maps (**Fig. 3d**); (iii) importantly, because loop extrusion is a *cis*-acting

141 process, pairs of Rec8 sites at increasing separations naturally have lower contact frequency
142 (**Fig. 3e**).
143
144 Simulations also highlight the stochasticity of loop positions across the cell population, with most
145 barriers (73%) unoccupied by an extruder, and extruders paused with barrier elements on both
146 sides only a minority of the time (15%) in the best fitting models (**Extended Data Fig. 6c**).
147 Because of this, the majority (65%) of extruded loops cross over Rec8 sites, consistent with an
148 average loop size roughly twice the average distance between Rec8 ChIP peaks (26 kb versus
149 12 kb, **Extended Data Fig. 6d**), and remarkably consistent with estimates made using EM
150 (~20kb[36]). Most strikingly—despite the prominence of Rec8-dependent grid-like features in the
151 experimental data (**Fig. 2c**)—our simulations indicate that Rec8 sites are not always occupied
152 by extruding cohesins and thus are present at the meiotic chromosome core in only a subset of
153 cells, as inferred previously[38].
154
155 The range of loop extrusion parameters we explored encompasses the situation where Rec8
156 sites always halt extrusion and *cis*-loops are formed between each consecutive Rec8 site.
157 However, simulations with these parameters have quantitatively poor fits with experimental
158 maps (**Fig. 3d-e, ii**): the bend in *P(s)* comes too early to recapitulate experimental *P(s)*, and
159 Rec8-Rec8 contacts are much too strong. The poor fit of such 'direct-bridging' simulations
160 underscores the conclusion that only a fraction of Rec8 sites are occupied in a given cell, and
161 argues that cohesin-dependent *cis*-loops must link regions that are not primary Rec8 binding
162 sites in order to provide compaction without making Rec8-Rec8 enrichments overly strong.
163
164 A crucial prediction of our loop extrusion simulations is that depletion of extruders in meiosis
165 would lead to both decompaction and loss of the grid-like pattern of Hi-C interactions. When we
166 repeated our fitting procedure for *rec8*Δ, the best fits were for simulations with either no, or very
167 few, extruded loops (**Extended Data Fig. 5e**). The lack of compaction in these simulations
168 (**Extended Data Fig. 5a**) is consistent with previous EM showing decompacted chromatids in
169 *rec8*Δ[3]. Such joint consistency between Hi-C and imaging data further supports loop extrusion
170 as a mechanism underlying assembly of the cohesin-rich core and contributing to chromosomal
171 compaction in meiosis. Our simulations also open the possibility that overly-shortened axes
172 observed upon Wapl[39,40] and Pds5[41] depletion may reflect heightened extruder processivity[42]
173 upon which shortened SCs are assembled, and predict that such perturbations would cause a
174 rightward shift in the *P(s)* shoulder measured via Hi-C (**Extended Data Fig. 5c**).
175

To investigate how homologue synapsis affects chromosome conformation, we assayed pachytene cells in the absence of Zip1, the transverse filament of the SC[4], and Hop1, an axial element required for Zip1 loading[6] (**Fig. 4a,b**). Both *zip1*Δ and *hop1*Δ Hi-C maps retained the Rec8-dependent punctate interactions (**Fig. 4b, Extended Data Fig. 2b,c**), and displayed compaction relative to G1 or *rec8*Δ, but with the *P(s)* shoulder shifted left relative to *ndt80*Δ (**Fig. 4c**). Attempts to model the known *zip1*Δ and *hop1*Δ defects in chromosome synapsis simply by removing interhomologue crosslinks from best-fitting *ndt80*Δ simulations did not recapitulate the *P(s)* shift observed experimentally (**Extended Data Fig. 5f**), consistent with the suggestion that interhomologue contacts make only a minor contribution within meiotic Hi-C maps[24]. Instead, best-fitting simulations had shifts towards slightly lower processivity and larger separation, consistent with less axial compaction relative to the *ndt80*Δ control (**Fig. 4e**). Interestingly, subtelomeric regions no longer displayed a distinct *P(s)* in *zip1*Δ and *hop1*Δ (**Fig. 4d**), suggesting that chromosome compaction at chromosome termini is regulated differentially.

Discussion

Our analysis of meiotic chromosome organisation reconciles the function and localisation of factors thought to shape meiotic chromosomes with their 3D organisation. Crucially, we have demonstrated the centrality of cohesin function and localisation for meiotic *cis*-loop formation—formally demonstrating the link between preferential positioning of Rec8 along the genome[28,35] and the inference that these loci come into close proximity based on the localization of Rec8 to the chromosomal axes[3].

Rec8 positioning correlates with sites of converging transcription[35]. We favour the view that transcription acts as a barrier to cohesin-dependent loop extrusion in meiosis, rather than as a motive force as previously proposed[35], consistent with transcription-independent compaction by cohesin in mammalian interphase[43] and direct observation of extrusion by the related SMC condensin *in vitro*[44]. Nevertheless, whether barriers arise directly from Pol2 binding, or indirectly via other axis proteins, remains to be determined. Loop extrusion would also be expected to be blocked by large DNA-protein complexes[29], such as the kinetochore—consistent with the paucity of Rec8-dependent loops that span the centromere.

Our simulations also help reveal a nuanced picture of meiotic chromosome assembly: loops are, on average, larger than the inter-Rec8 peak distance, and more than half of the loop bases are not associated with preferred sites of Rec8 binding. Moreover, it is likely that loop sizes and positions vary widely from one cell to another, making classifications of genomic regions as ‘axis’ or ‘loop’ a great oversimplification. Despite using the simplifying assumption that all

211 barriers had equal strength, our simulations generated interaction maps closely resembling
212 experimental Hi-C maps. This agreement furthers the case for loop extrusion as a general
213 mechanism[19–21,24,29,45–48] that is flexibly employed and regulated in interphase, mitosis, and
214 meiosis.
215
216 Our results point to interesting similarities and differences between yeast mitosis and meiosis.
217 In both systems, chromosome arm compaction is dependent on the corresponding cohesin
218 kleisin subunit and consistent with *cis*-loops generated via loop extrusion. The presence of focal
219 interactions in meiosis but not in mitosis remains intriguing, however, and suggests the influence
220 of additional components. Indeed, loop extrusion simulations require barriers to agree with
221 experimental meiotic Hi-C maps. Nevertheless, our observations enable us to rule out the axial
222 element, Hop1, the SC transverse filament, Zip1, and the process of homologous recombination
223 mediated by Spo11, Sae2, and Dmc1 (unpub. obs.) as important for the generation of such
224 patterns.
225
226 It is notable that the meiotic grid-like pattern of interactions observed between Rec8 sites is
227 reminiscent of the patterns seen between oriented CTCF sites in mammalian interphase[13,25].
228 Interestingly, the meiotic patterns are even more reminiscent of the Hi-C patterns observed in
229 interphase mammalian cells upon depletion of the cohesion unloader, Wapl[32,43], wherein
230 "vermicelli"-like chromatids arise with a cohesin-rich backbone[49], suggesting that cohesin
231 metabolism may be altered in meiosis via modulation of the cohesin regulators.
232
233 Our results also reveal how the interplay between the synapsis components, Hop1 and Zip1,
234 influences chromosome morphology. That Hop1 and Zip1 are both required to increase
235 chromosome compaction at pachytene likely points at their joint role in promoting synapsis[4,6],
236 and supports the view that synapsis itself modulates axial compaction. Interestingly, whilst Zip1
237 binds largely uniformly along the arms of pachytene chromosomes[50], subtelomeres and short
238 chromosomes display an increase in short-range contacts and an earlier shoulder in *P(s)*,
239 consistent with smaller loops or less compression of spacers between loops in these regions,
240 and therefore less axial compaction. Because such differences correlate with disproportionate
241 retention of Hop1 in these regions[50] and diminished efficiency of synapsis[51], it is possible that
242 Hop1 impedes the pathway whereby Zip1 imposes additional compaction upon synapsis.
243 Nevertheless, it is unclear whether Zip1 mediates this effect by modifying loop extrusion
244 dynamics, or via a distinct process of axial compression, as has been argued for higher-
245 eukaryote mitotic chromosome compaction[20]. Given the influence that chromosome structure
246 has over so many aspects of meiosis, teasing apart these mechanisms is of great future interest.

247

248 # Acknowledgements & Contributions

249 SAS and MJN planned the study, performed wet-lab work and data analysis. GF and KSP
250 developed polymer simulations and performed data analysis. SAS, GF, JB, KSP and MJN
251 discussed results and wrote the manuscript. We thank Tim Cooper for deploying the HiC Pro
252 installation, Scott Keeney and Franz Klein for sharing *S. cerevisiae* strains, Svetlana Lyalina for
253 assistance with QB3 GPUs, Anton Goloborodko for suggesting the use of *looplib*, and Nezar
254 Abdennur for feedback.

255 # Data & Code Availability

256 All processed Hi-C matrices are publicly accessible via the interactive HiGlass[52] viewer. Live
257 web links are provided with each figure. Raw sequence reads will be made publicly accessible
258 via the SRA repository upon final publication. Code for data analysis is either already publicly
259 available online or will be made available on request or via Github upon final publication.

260 # Figure Legends

261 **Figure 1. Chromosome conformation during yeast meiosis.**

262 **a.** Cells were collected during meiosis at indicated timepoints and analysed by Hi-C. At 0h the
263 cells are in G1. Representative Hi-C contact maps of chromosomes 6, 11, and 7 plotted at 5 kb
264 resolution. Centromeres, telomeres and arm fold-back at the centromere are indicated by blue,
265 red and grey arrows, respectively, and axial compaction by the width of the main diagonal
266 relative to the fixed-width black clamp. For interactive HiGlass[52] views see:
267 http://higlass.pollard.gladstone.org/app/?config=Z5iwKpjzQpePCXXyvuYGeQ
268 **b.** Meiotic entry assessed by FACS; at 4 h, the majority of cells show a 4C peak indicating
269 completion of DNA replication.
270 **c.** Meiotic progression was monitored by quantification of nuclear divisions determined by DAPI
271 staining. Around 4 h, cells start to undergo meiotic divisions I and II. The majority of cells
272 undergo meiotic divisions between 4 and 8 h, indicating the degree of heterogeneity within the
273 cell population.

d. *Upper panels*: Average *trans* centromere-centromere contact maps. *Lower panels*: *trans* telomere-telomere contact maps. *Right*: ratio of *cis* to total contact frequency.

e. Intra-arm contact probability versus genomic distance, *P(s),* indicating the emergence (*left*) and disappearance (*right*) of chromosome arm compaction during meiosis. Shaded area bounded above and below by the two *ndt80*Δ 8h replicates.

f. Meiosis was induced in *ndt80*Δ cells for 8h and meiotic entry was checked by monitoring DNA replication by FACS.

g. *ndt80*Δ cells were grown for 8h in sporulation media and analysed by Hi-C (*left*). Log2 ratio of *ndt80*Δ cells 8h over G1 (*right*). Centromeres and telomeres are indicated by blue and red arrows, respectively, and axial compaction by a black clamp.

h. *Left*: Contact probability of individual chromosome arms stratified by length. *Right*: Contact probability stratified by the distance from the telomere.

Figure 2. Emergence of a Rec8-dependent grid of punctate interactions in meiosis

a. Hi-C contact maps of chromosome 11 for the indicated genotypes plotted at 2 kb bin resolution, showing near-diagonal interactions. Wild type timepoints as in **Fig. 1a**. **Lower panels**: log2(insulation); cis/total ratio, Rec8 ChIP-seq[28], all binned at 2kb. Insulation and cis/total calculated from *ndt80*Δ maps. Positions of Rec8 sites indicated as green circles. Genome-wide cis/total (Spearman's R=0.62, P<1e-10) and insulation (R= -0.23, P<1e-10, insulation window = 20 kb) profiles are correlated with Rec8 occupancy.

b. Zoom-in into contact maps on chromosome 11 (0-200kb) of wt-4h and *ndt80*Δ (top) and *rec8*Δ (*bottom left*). Contact probability versus genomic distance, *P(s)*, for G1(*ndt80Δ-0h*) and *ndt80*Δ and *rec8*Δ (*bottom right*). Data shown is the average (n=2) except for wt-4h. Rec8 peak sites called from ChIP-seq data[28] are indicated in green. For an interactiveview see: http://higlass.pollard.gladstone.org/app/?config=Twrh61jGT4SIxotaguTIJg

c. Simplified illustration of how a grid of peaks on a Hi-C map can emerge between Rec8 sites either by transitive contacts between adjacent loops, or by loops that skip over adjacent sites. Experimentally observed grids extend much further than separation=2 (**Extended Data Fig. 4c**)

d. Cis/total ratios for Rec8 (green) and nonRec8 (grey) sites for indicated datasets.

e. Contact frequency versus distance between Rec8-Rec8 sites (green), Rec8-nonRec8 sites (light green) and nonRec8-nonRec8 sites (green).

f. Log2 ratio of contact frequency between adjacent Rec8-sites (separation=1) compared to average cis interactions.

g. Log2 ratio of contact frequency centered at Rec8 sites compared to average cis interactions.

307 In *ndt80*Δ, Rec8 sites show: elevated cis/total frequency (0.85 versus 0.77), elevated pairwise
308 contact frequency (~2-fold at 20 kb), and mild insulation. These distinctions are similar in wild
309 type pachytene (4h) yet absent in G1 (*ndt80Δ-0h*) or in *rec8*Δ.

310 **Figure 3. Model for meiotic chromosome compaction in prophase.**

311 **a.** In simulations, yeast chr13 was represented as a polymer fiber confined to the nucleus
312 subject to additional meiosis-specific constraints. These include: extruded loops, sister
313 crosslinks, and homolog crosslinks (**Methods**). Barriers to extruded loops were placed at Rec8
314 sites[28]. We imposed inter-sister and inter-homologue crosslinks at sites of extruded loop bases
315 in order to approximate the paired arrangement of homologues at pachytene (**Extended Data**
316 **Fig. 6**). For each set of extruded loop parameters (*processivity, separation,* and *barrier*
317 *strength*), conformations were collected and used to generate simulated contact maps. These
318 were then compared with experimental contact maps via the combined average fold
319 discrepancy with *P(s)* curves for Rec8-Rec8, Rec8-non, and non-non bin pairs at 2 kb
320 resolution.
321 **b.** Goodness-of-fit for indicated barrier strengths over coarse grids of processivity and
322 separation demonstrate that intermediate barrier strengths are required to agree with
323 experimental *ndt80*Δ Hi-C maps.
324 **c.** Goodness-of-fit for a fine grid of processivity versus separation at barrier strength 0.95. Best-
325 fitting models had separation ~32kb and processivity ~76kb, corresponding to ~60% coverage
326 of the genome by extruded loops of average length 26kb.
327 **d.** From *left* to *right*: contact maps for chr13 for *ndt80Δ*, and simulations with (i) best-fitting
328 parameters, (ii) relatively stable loops between neighboring Rec8 sites, and (iii) no barriers.
329 **e.** P(s) split by Rec8-Rec8, Rec8-non, and non-non, as in **Fig. 2D**.
330 **f.** Conformations for best-fitting simulations, which highlight: (*left)* one chromatid colored from
331 start (red) to end (blue); *(right*) extruders (yellow), extrusion barriers (red), and extruders paused
332 at barriers (orange).

333 **Figure 4. Hop1 and Zip1-dependent compaction of Rec8-dependent loops.**

334 **a.** *Top*: Hi-C maps for *hop1*Δ and *zip1*Δ (plotted as in **Fig. 1a**). *Bottom*: Log2 ratio of hop1Δ over
335 *ndt80*Δ (as in **Fig. 1g**). For interactive views of the full genome, see
336 http://higlass.pollard.gladstone.org/app/?config=TTBGu5DDR0SHAa09zrjTXA
337 **b.** Hi-C contact maps of chromosome 11 for *hop1*Δ and *zip1*Δ plotted at 2kb bin resolution,
338 showing near-diagonal interactions, as in **Fig. 2a**.

c. Contact probability versus genomic distance for G1, *ndt80*Δ, *hop1*Δ, *zip1*Δ. Shaded area bounded above and below by *ndt80*Δ replicas. Average between two replicas for *zip1*Δ and one sample for G1 and *hop1*Δ are shown.

d. Contact probability over genomic distance averaged over all chromosome arms stratified by distance from the telomere.

e. Goodness-of-fit for simulations without homolog crosslinks with a fine grid of processivity versus separation at barrier strength 0.95 *zip1*Δ and *hop1*Δ.

f. Model of meiotic chromosome compaction: Rec8-dependent loop formation leads to initial chromosome arm compaction and emergence of a grid-like pattern of Hi-C interactions that jointly agrees with a mechanism of loop extrusion including barrier elements. We suggest that transcription could impose such barriers. Hop1 and Zip1 are dispensable for this step, but are required for synapsis, where additional compaction occurs differentially along chromosome arms.

Extended Data Fig. 1

a-d. Results from a replicate timecourse, collected and characterized independently of the timecourse in Fig. 1.

a. Hi-C maps, plotted as in Fig. 1a.

b. FACS as in Fig. 1b.

c. DAPI as in Fig. 1c.

d. *P(s)* as in Fig. 1e.

e. *P(s)* for chromosomes stratified by size for *ndt80*Δ-0h, *ndt80*Δ-8h. Short chromosomes display relatively elevated *P(s)* at short distances, and an earlier shoulder.

f. *Left*: *P(s)* for individual chromosome arms, stratified by size for wt-4h. Short arms display relatively elevated *P(s)* at short distances, and an earlier roll-over. *Right*: Intra-arm *P(s)* stratified by the distance from the telomere for wt-4h, averaged across all chromosomes. Telomere-proximal regions display elevated *P(s)* at short distances.

g. Intra-arm *P(s)* stratified by the distance from the centromere for G1 (*ndt80*Δ-0h), *wt*-4h, *ndt80*Δ-8h, averaged across all chromosomes.

h. Contact probability of single chromosome arms for *ndt80*Δ-8h.

Extended Data Fig. 2

a. Average *trans* centromere-centromere contact maps for indicated data sets.

b. Average *cis* centromere-centromere contact maps for indicated data sets. Note the loss of the folding back in meiosis, and how the intra-arm enrichment is insulated at centromeres in meiosis.

Extended Data Fig. 3

a. Average *trans* telomere-telomere contact maps for indicated datasets.

b. Average telomere-telomere contact maps between the two telomeres of the same chromosome.

c. Average contact map around each telomere in *cis.*

Extended Data Fig. 4

a. *Left*: Hi-C contact maps of *rec8*Δ *ndt80*Δ. Chromosomes 6, 11 and 7 are shown as representatives for the whole genome. *Right*: Log2 Hi-C ratio maps of *rec8*Δ *ndt80*Δ / *ndt80*Δ. Plotted as in Fig. 1g.

b. Log2 observed over expected contact frequency at Rec8-Rec8 peak pairs as a function of separation across datasets.

c. Log2 observed over expected contact frequency +/-8kb around Rec8-Rec8 peak pairs at the indicated separations.

Together, **b-c** demonstrate that Rec8-Rec8 enrichments are strongest between adjacent sites, decrease between non-adjacent sites with increasing genomic separation, and are absent in *trans*. Equally important, these meiotic features are lost in *rec8*Δ. As for mammalian interphase, this observation in meiosis argues for a *cis*-acting process underlying the formation of focal interactions between Rec8 sites.

d. cis/total as a function of distance along the chromosomal arm, Rec8 sites marked in green.

Extended Data Fig. 5

a. Representative conformation for the indicated parameter sets. As in **Fig. 3f,** one chromatid from a homologous quartet of chromatids coloured from start to end according to the spectrum; other three coloured in grey.

b. For the same three conformations, positions of Rec8 sites indicated with red spheres, positions of extruded loop bases in yellow, and extruders overlapping a Rec8 site in orange. Note the stable loops between neighbouring Rec8 sites creates a very elongated chromatid (ii). Also note the majority of Rec8 sites are unoccupied in (iii), despite the self-assembly of two axial cores and a strong brush. Finally, note very dispersed chromosomes in (iv), consistent with EM[3] for *rec8*Δ.

c. Contact frequency versus distance, *P(s),* for indicated simulations. Note that the loss of the shoulder in *P(s)* in the case of full extruder depletion mirrors the difference between experimental *ndt80*Δ and *rec8*Δ Hi-C maps. Simulations with increased processivity predict that *P(s)* would shift rightward if unloading was impaired, as could happen in *waplΔ.* Conversely, if

407 unloading was enhanced, simulations with decreased processivity indicate a leftward shift in
408 P(s), until the absence of extruders.
409 **d.** Goodness-of-fit for a fine grid of processivity versus separation at barrier strength 0.90. The
410 best-fit occurs at similar processivity and separation as for barrier strength 0.95 shown in **Fig.**
411 **3c**, but with slightly lower goodness-of-fit.
412 **e.** Goodness-of-fit to *rec8Δ* data for simulations with the indicated barrier strengths (in grey:
413 0.00, 0.75, 0.90, 0.95, 0.99, 1.00) over coarse grids of processivity and separation demonstrates
414 that the best fits have few if any extruded loops, regardless of barrier strength.
415 **f.** *P(s)* curves for simulations with sisters and homologs with the best-fitting parameters for
416 *ndt80Δ-8h* maps compared to P(s) for simulations with sisters only show that simply removing
417 homolog tethering does not recapitulate the sort of shifted P(s) seen experimentally in *zip1*Δ Hi-
418 C.

419 **Extended Data Fig. 6**

420 **a.** Simulated contact maps for the indicated region of chr13 for: (i) best-fitting simulations, (ii)
421 simulations with relatively stable loops between neighboring Rec8 sites (barrier strength=1 and
422 high processivity), and (iii) no barriers, as in **Fig. 2d.**
423 **b.** Simulated ChIP-seq profiles for the indicated region of chr13. Best-fitting simulations (i)
424 display occupancy well below 100% at Rec8 sites. Simulations with stable loops (ii) display
425 highly occupied Rec8 sites. Simulations without barriers (iii) have homogenous Rec8 occupancy
426 across the genome.
427 **c.** Positions of extruded loops (arcs) sister crosslinks (solid black lines) and homolog crosslinks
428 (dashed lines) for four chromatids in two separate cells, showing how the simulated Hi-C maps
429 and ChIP-seq profiles emerge from the stochastic positioning of extruded loops from cell-to-cell.
430 For statistics, see **Supplementary Table S1**.
431 **d.** Histogram of extruded loop lengths for indicated parameters (i, ii, iii).
432

433 # Tables

434
435 **Table 1. *S. cerevisiae* strains used in this study**

Strain name	Genotype
MJ6	*ho::LYS2/", lys2/", ura3/", arg4-nsp/", leu2::hisG/", his4X::LEU2/", nuc1::LEU2/"*

SSY14	*ho::LYS2/'', lys2/'', ura3/'', arg4-nsp/'', leu2::hisG/'', his4X::LEU2/'', nuc1::LEU2/'', ndt80Δ::LEU2/''*
SSY20	*ho::LYS2/'', lys2/'', ura3/'', arg4-nsp/'', leu2::hisG/'', rec8Δ::KanMX4/'', ndt80Δ::LEU2/''*
SSY25	*ho::LYS2/'', lys2/'', ura3/', arg4-nsp/'', leu2::hisG/'', his4X::LEU2/'', nuc1::LEU2/'', zip1::LEU2/'', ndt80Δ::LEU2/''*
SSY49	ho::LYS2/'', lys2/'', ura3/'', arg4-nsp/'', leu2::hisG/'', nuc1::LEU2/'', his4X::LEU2/'', hop1::LEU2/'', ndt80Δ::LEU2/''
SSY58	ho::hisG/", lys2/'', ura3/'', leu2::hisG/'', nuc1::LEU2/'', arg4-nsp/'', rec8::KanMX/'', ndt80Δ::LEU2/''

Table 2. Hi-C Libraries

Name	**mutations**	**Sample name**	**valid pairs (M)**
Main figures			
wt-0h (G1)		HiC_MJ6_wt_2A_0h	14.5
wt-2h		HiC_MJ6_wt_2A1_2h	27.6
wt-3h		HiC_MJ6_wt_2A_3h	24.1
wt-4h		HiC_MJ6_wt_2A_4h	28
wt-5h		HiC_MJ6_wt_2A1_5h	27.6
wt-6h		HiC_MJ6_wt_2A1_6h	27.6
wt-8h		HiC_MJ6_wt_2A3_8h	19
*rec8*Δ	*rec8*Δ *ndt80*Δ	average	
*rec8*Δ replica 1	*rec8*Δ *ndt80*Δ	HiC_SSY20_ndt80Drec8D_1A2_8h	39.3
*rec8*Δ replica 2	*rec8*Δ *ndt80*Δ	HiC_SSY58_ndt80Drec8D_2A_8h	20.2
*ndt80*Δ	*ndt80*Δ	average, 8h	
G1	*ndt80*Δ	HiC_SSY14_ndt80D_1A2_0h	36
*ndt80*Δ-4h	*ndt80*Δ	HiC_SSY14_ndt80D_1A_4h	11.9
*ndt80*Δ replica 1	*ndt80*Δ	HiC_SSY14_ndt80D_1A1_8h	22.9
*ndt80*Δ replica 2	*ndt80*Δ	HiC_SSY14_ndt80D_2A2_8h	37
*zip1*Δ	*zip1*Δ *ndt80*Δ	average	
*zip1*Δ replica 1	*zip1*Δ *ndt80*Δ	HiC_SSY25_ndt80Dzip1D_1B2_8h	22.7

*zip1*Δ replica 2	*zip1*Δ *ndt80*Δ	HiC_SSY25_ndt80Dzip1D_2A_8h	28.6
*hop1*Δ	*hop1*Δ *ndt80*Δ	hop1 ndt80	
*hop1*Δ replica1	*hop1*Δ *ndt80*Δ	HiC_SSY49_ndt80Dhop1D_1A_8h	32.8
Supplementary figures			
wt-2h		HiC_MJ6_wt_3A_2h	22.5
wt-3h		HiC_MJ6_wt_3A_3h	19.8
wt-4h		HiC_MJ6_wt_3A_4h	16.7
wt-6h		HiC_MJ6_wt_3A_6h	37.6

Table 3. Overview of proteins described in this study

Protein	Description
Ndt80	Transcription factor required for exit from pachytene
Rec8	Meiosis-specific kleisin subunit of cohesin
Hop1	Axial element of the synaptonemal complex
Zip1	Transverse filament of the synaptonemal complex

References

1. Zickler, D. & Kleckner, N. Meiotic chromosomes: integrating structure and function. *Annu Rev Genet* **33**, 603-754 (1999).
2. Gray, S. & Cohen, P. E. Control of Meiotic Crossovers: From Double-Strand Break Formation to Designation. *Annu Rev Genet* (2016).
3. Klein, F. et al. A central role for cohesins in sister chromatid cohesion, formation of axial elements, and recombination during yeast meiosis. *Cell* **98**, 91-103 (1999).
4. Sym, M., Engebrecht, J. A. & Roeder, G. S. ZIP1 is a synaptonemal complex protein required for meiotic chromosome synapsis. *Cell* **72**, 365-378 (1993).
5. Smith, A. V. & Roeder, G. S. The yeast Red1 protein localizes to the cores of meiotic chromosomes. *J Cell Biol* **136**, 957-967 (1997).
6. Hollingsworth, N. M., Goetsch, L. & Byers, B. The HOP1 gene encodes a meiosis-specific component of yeast chromosomes. *Cell* **61**, 73-84 (1990).
7. Maleki, S., Neale, M. J., Arora, C., Henderson, K. A. & Keeney, S. Interactions between Mei4, Rec114, and other proteins required for meiotic DNA double-strand break formation in Saccharomyces cerevisiae. *Chromosoma* **116**, 471-486 (2007).
8. Li, J., Hooker, G. W. & Roeder, G. S. Saccharomyces cerevisiae Mer2, Mei4 and Rec114 form a complex required for meiotic double-strand break formation. *Genetics* **173**, 1969-1981 (2006).
9. Dekker, J., Rippe, K., Dekker, M. & Kleckner, N. Capturing chromosome conformation. *Science* **295**, 1306-1311 (2002).

10. Bonev, B. & Cavalli, G. Organization and function of the 3D genome. *Nat Rev Genet* **17**, 661-678 (2016).
11. Merkenschlager, M. & Nora, E. P. CTCF and Cohesin in Genome Folding and Transcriptional Gene Regulation. *Annu Rev Genomics Hum Genet* **17**, 17-43 (2016).
12. Dekker, J. & Mirny, L. The 3D Genome as Moderator of Chromosomal Communication. *Cell* **164**, 1110-1121 (2016).
13. Fudenberg, G., Abdennur, N., Imakaev, M., Goloborodko, A. & Mirny, L. A. Emerging Evidence of Chromosome Folding by Loop Extrusion. *Cold Spring Harb Symp Quant Biol* **82**, 45-55 (2017).
14. Jin, Q., Trelles-Sticken, E., Scherthan, H. & Loidl, J. Yeast nuclei display prominent centromere clustering that is reduced in nondividing cells and in meiotic prophase. *J Cell Biol* **141**, 21-29 (1998).
15. Hayashi, A., Ogawa, H., Kohno, K., Gasser, S. M. & Hiraoka, Y. Meiotic behaviours of chromosomes and microtubules in budding yeast: relocalization of centromeres and telomeres during meiotic prophase. *Genes Cells* **3**, 587-601 (1998).
16. Goloborodko, A., Marko, J. F. & Mirny, L. A. Chromosome Compaction by Active Loop Extrusion. *Biophys J* **110**, 2162-2168 (2016).
17. Gibcus, J. H. et al. A pathway for mitotic chromosome formation. *Science* **359**, (2018).
18. Kakui, Y., Rabinowitz, A., Barry, D. J. & Uhlmann, F. Condensin-mediated remodeling of the mitotic chromatin landscape in fission yeast. *Nat Genet* **49**, 1553-1557 (2017).
19. Lazar-Stefanita, L. et al. Cohesins and condensins orchestrate the 4D dynamics of yeast chromosomes during the cell cycle. *EMBO J* **36**, 2684-2697 (2017).
20. Naumova, N. et al. Organization of the mitotic chromosome. *Science* **342**, 948-953 (2013).
21. Schalbetter, S. A. et al. SMC complexes differentially compact mitotic chromosomes according to genomic context. *Nat Cell Biol* **19**, 1071-1080 (2017).
22. Xu, L., Ajimura, M., Padmore, R., Klein, C. & Kleckner, N. NDT80, a meiosis-specific gene required for exit from pachytene in Saccharomyces cerevisiae. *Mol Cell Biol* **15**, 6572-6581 (1995).
23. Nagano, T. et al. Cell-cycle dynamics of chromosomal organization at single-cell resolution. *Nature* **547**, 61-67 (2017).
24. Muller, H. et al. Characterizing meiotic chromosomes' structure and pairing using a designer sequence optimized for Hi-C. *Mol Syst Biol* **14**, e8293 (2018).
25. Rao, S. S. P. et al. A 3D map of the human genome at kilobase resolution reveals principles of chromatin looping. *Cell* **159**, 1665-1680 (2014).
26. Nora, E. P. et al. Spatial partitioning of the regulatory landscape of the X-inactivation centre. *Nature* **485**, 381-385 (2012).
27. Dixon, J. R. et al. Topological domains in mammalian genomes identified by analysis of chromatin interactions. *Nature* **485**, 376-380 (2012).
28. Ito, M. et al. Meiotic recombination cold spots in chromosomal cohesion sites. *Genes Cells* **19**, 359-373 (2014).
29. Fudenberg, G. et al. Formation of Chromosomal Domains by Loop Extrusion. *Cell Rep* **15**, 2038-2049 (2016).
30. Schwarzer, W. et al. Two independent modes of chromatin organization revealed by cohesin removal. *Nature* **551**, 51-56 (2017).
31. Rao, S. S. P. et al. Cohesin Loss Eliminates All Loop Domains. *Cell* **171**, 305-320.e24 (2017).
32. Wutz, G. et al. Topologically associating domains and chromatin loops depend on cohesin and are regulated by CTCF, WAPL, and PDS5 proteins. *EMBO J* **36**, 3573-3599 (2017).
33. Conrad, M. N., Lee, C. Y., Wilkerson, J. L. & Dresser, M. E. MPS3 mediates meiotic bouquet formation in Saccharomyces cerevisiae. *Proc Natl Acad Sci U S A* **104**, 8863-8868 (2007).
34. Trelles-Sticken, E., Adelfalk, C., Loidl, J. & Scherthan, H. Meiotic telomere clustering requires actin for its formation and cohesin for its resolution. *J Cell Biol* **170**, 213-223 (2005).

35. Sun, X. et al. Transcription dynamically patterns the meiotic chromosome-axis interface. *Elife* **4**, (2015).
36. Møens, P. B. & Pearlman, R. E. Chromatin organization at meiosis. *Bioessays* **9**, 151-153 (1988).
37. Marko, J. F. & Siggia, E. D. Polymer models of meiotic and mitotic chromosomes. *Mol Biol Cell* **8**, 2217-2231 (1997).
38. Blat, Y. & Kleckner, N. Cohesins bind to preferential sites along yeast chromosome III, with differential regulation along arms versus the centric region. *Cell* **98**, 249-259 (1999).
39. Crawley, O. et al. Cohesin-interacting protein WAPL-1 regulates meiotic chromosome structure and cohesion by antagonizing specific cohesin complexes. *Elife* **5**, e10851 (2016).
40. Challa, K., Lee, M.-S., Shinohara, M., Kim, K. P. & Shinohara, A. Rad61/Wpl1 (Wapl), a cohesin regulator, controls chromosome compaction during meiosis. *Nucleic Acids Res* **44**, 3190-3203 (2016).
41. Jin, H., Guacci, V. & Yu, H.-G. Pds5 is required for homologue pairing and inhibits synapsis of sister chromatids during yeast meiosis. *J Cell Biol* **186**, 713-725 (2009).
42. Petela, N. J. et al. Scc2 Is a Potent Activator of Cohesin's ATPase that Promotes Loading by Binding Scc1 without Pds5. *Mol Cell* **70**, 1134-1148.e7 (2018).
43. Haarhuis, J. H. I. et al. The Cohesin Release Factor WAPL Restricts Chromatin Loop Extension. *Cell* **169**, 693-707.e14 (2017).
44. Ganji, M. et al. Real-time imaging of DNA loop extrusion by condensin. *Science* (2018).
45. Sanborn, A. L. et al. Chromatin extrusion explains key features of loop and domain formation in wild-type and engineered genomes. *Proc Natl Acad Sci U S A* **112**, E6456-65 (2015).
46. Nasmyth, K. Disseminating the genome: joining, resolving, and separating sister chromatids during mitosis and meiosis. *Annu Rev Genet* **35**, 673-745 (2001).
47. Goloborodko, A., Imakaev, M. V., Marko, J. F. & Mirny, L. Compaction and segregation of sister chromatids via active loop extrusion. *Elife* **5**, (2016).
48. Alipour, E. & Marko, J. F. Self-organization of domain structures by DNA-loop-extruding enzymes. *Nucleic Acids Res* **40**, 11202-11212 (2012).
49. Tedeschi, A. et al. Wapl is an essential regulator of chromatin structure and chromosome segregation. *Nature* **501**, 564-568 (2013).
50. Subramanian, V. V. et al. Persistent DNA-break potential near telomeres increases initiation of meiotic recombination on short chromosomes. *Biorxiv* (2017).
51. Thacker, D., Mohibullah, N., Zhu, X. & Keeney, S. Homologue engagement controls meiotic DNA break number and distribution. *Nature* **510**, 241-246 (2014).
52. Kerpedjiev, P. et al. HiGlass: web-based visual exploration and analysis of genome interaction maps. *Genome Biol* **19**, 125 (2018).

554 # Methods

555 **Yeast strains and cell culture growth.**

556 Strains used in this study were derived from SK1 and are listed in Table 1.

557 **Monitoring meiotic progression by flow cytometry and quantification of nuclear divisions**

558 Cells were fixed in 70% EtOH, digested with 1 mg/ml RNAse (10 mM Tris-HCl pH 8.0, 15 mM
559 NaCl, 10 mM EDTA pH 8.0) for 2 h at 37 ˚C, 800 rpm and subsequently treated with 1 mg/ml
560 Proteinase K in 50 mM Tris-HCl pH 8.0 at 50 ˚C, 800 rpm for 30 min for analysis by FACS. Cells
561 were then washed in 50 mM Tris-HCl pH 8.0 and stained in the same buffer with 1 uM Sytox
562 green overnight in the fridge. FACS profiles were plotted with R using the library *hwglabr2*
563 (https://github.com/hochwagenlab/hwglabr2). Fixed cells were also used for quantification of
564 nuclear divisions by spreading onto a microscope slide, mounting with Fluoroshield containing
565 DAPI followed by analysis with a Zeiss Scope.A1 microscope.

566 **Hi-C library preparation**

567 The Hi-C protocol used was amended from[1] by ~5-fold reduction in all materials and volumes.
568 Briefly, *S. cerevisiae* diploid cells were synchronised in G1 by growth at 30 ˚C for ~15 h in 30
569 ml YPA (1% Yeast extract, 2% Peptone, 1% K-acetate) to OD600 of ~4, harvested, washed,
570 and resuspended in prewarmed sporulation medium (2% KAc with 0.2x nutritional supplements)
571 before fixing 5 ml aliquots (20-30 ODs) of relevant timepoints with formaldehyde at 3% final
572 concentration for 20 min at 30 °C, 250 rpm, then quenched by incubating with a final
573 concentration of 0.35 M Glycine (2x the volume of Formaldehyde added) for an additional 5
574 minutes. Cells were washed with water, split into two samples and stored at -80˚C ready for
575 library preparation. Cells were thawed, washed in spheroplasting buffer (SB, 1 M Sorbitol, 50
576 mM Tris pH 7.5) and digested with 100 ug/ml 100T Zymolyase in SB containing 1% beta-
577 Mercaptoethanol for 15-20 min at 35 ˚C. Cells were washed in restriction enzyme buffer,
578 chromatin was solubilised by adding SDS to 0.1% and incubating at 65 ˚C for 10 minutes.
579 Excess SDS was quenched by addition of Triton X100 to 1%, and chromatin was incubated with
580 2.07U/ul of *Dpn*II overnight at 37 ˚C. DNA ends were filled in with nucleotides, substituting dCTP
581 for biotin-14-dCTP using Klenow fragment DNA polymerase I at 37 ˚C for 2 h followed by
582 addition of SDS to 1.5% and incubation at 65 ˚C for 20 min to inactivate Klenow and further
583 solubilise the chromatin. The sample volume was diluted 15-fold, crosslinked DNA ends ligated
584 at 16 ˚C for 8 h using 0.024U/ul of T4 DNA ligase, and crosslinks reversed by overnight
585 incubation at 65 ˚C in the presence of Proteinase K. DNA was precipitated with ethanol,

586 dissolved in TE and passed through an Amicon 30 kDa column. DNA was further purified by
587 phenol:chloroform:isoamylalcohol extraction and precipitated again before treating with
588 RNaseA at 37 ˚C for 1 h. Biotin was removed from unligated ends by incubation with T4 DNA
589 polymerase at 20˚C for 4 h and at 75 ˚C for 20 min for inactivation of the enzyme. DNA was
590 subsequently fragmented using a Covaris M220 (Duty factor 20%, 200 cycles/burst, 350s, 20
591 ˚C), and DNA ends were repaired and A-tailed using T4 DNA polymerase, T4 Polynucleotide
592 Kinase and Klenow fragment DNA polymerase I before isolating fragments of 100-250 bp using
593 a Blue Pippin (Sage). Biotinylated fragments were enriched using streptavidin magnetic beads
594 (C1) and NextFlex (Bioo Scientific) barcoded adapters were ligated while the DNA was on the
595 beads. Resulting libraries were minimally amplified by PCR and sequenced using paired end
596 42 bp reads on a NextSeq500 (Illumina; Brighton Genomics).

597 **Hi-C data processing and analysis**

598 Hi-C sparse matrices were generated at varying spatial resolutions using the Hi-C-pro pipeline[2],
599 using a customised S288c reference genome (*SK1Mod*, in which high confidence SK1-specific
600 polymorphisms were inserted in order to improve read alignment rates; manuscript in
601 preparation) and plotted using R Studio (version 1.0.44) after correcting for read depth
602 differences between samples. Raw read statistics are presented in **Table 2**. Repeat biological
603 samples gave broadly similar matrices and, unless indicated otherwise, were averaged to
604 improve their expected quantitative accuracy. As visual inspection indicated a number of
605 potential translocations in the SK1 strain as compared with the S288c reference genome, for
606 conservative downstream analyses, additional bins were masked if they contained potential
607 translocations. Such bins were identified if they either had values in *trans* at the level of the
608 median of the third diagonal in *cis*, or the maximum value in *trans* exceeded the maximum value
609 in *cis* for SSY14 for bins displaying these properties in either *ndt80*Δ*-0h* or in *ndt80*Δ*-8h* and for
610 MJ6 in *wt-0h* or *wt-4h*. chr1 was excluded from downstream analysis as few informative bins
611 remained after filtering potential translocations.
612
613 Average maps centered at centromeres and telomeres were calculated as in[3], ensuring that
614 collected patches for average centromere maps did not extend inter-chromosomally, and
615 collected patches for average telomere maps did not extend beyond centromeres or inter-
616 chromosomally. Contact frequency versus distance curves, *P(s),* were calculated from 2 kb
617 binned maps, with logarithmically-spaced bins in *s* (numutils.logbins, https://bitbucket.org /
618 mirnylab/mirnylib, start =2, end = max(binned arm lengths), N=50), and restricting the
619 calculation to bin pairs within chromosomal arms and excluding bins less than 20 kb from
620 centromeres or telomere (as in[3]), and normalized to the average value at 4 kb. *P(s)* stratified by

621 distance to telomeres was calculated using the combined distance to telomeres for each bin-
622 pair (as in[4]), and excluded bins-pairs where one bin was closer to a centromere than telomere
623 along that arm. Distance to centromeres, and *P(s)* stratified by this distance, was calculated
624 similarly. Log2 insulation profiles were calculated using a sliding diamond window (as in[5]) with
625 a +/-20 kb (+/-10 bins) extent; as in[6] downstream analyses were restricted to when there were
626 zero or one filtered bins in the sliding window. To calculate histograms of cis/total (**Fig. 2D**),
627 bins were defined as either Rec8 or non-Rec8. To calculate *P(s)* split by Rec8 bin-pair status,
628 each bin-pair (i.e. entry of the heatmap) was assigned as either Rec8-Rec8, Rec8-nonRec8, or
629 non-non (e.g. **Fig. 2E**). *P(s)* was then aggregated separately across chromosomes for these
630 three categories, similar to calculation of *P(s)* within and between TADs[7]. Average log2
631 observed/expected maps were calculated by first dividing by intra-arm *P(s)* and then averaging
632 together appropriate patches of Hi-C maps. Correlations between Rec8 occupancy from[8] and
633 insulation or cis/total profiles excluded chromosome 12 because the rDNA locus greatly alters
634 the insulation profile within the right arm of the chromosome.

635 **Polymer simulations**

636 Meiotic loop extrusion simulations begin with a generic polymer representation of the yeast
637 chromatin fiber similar to that used in previous models of yeast mitotic chromosomes[9], where
638 each 20 nm monomer represents 640 bp (~4 nucleosomes). We simulated the chromatin fiber
639 with excluded volume interactions and without topological constraints, using Langevin dynamics
640 in OpenMM, as in[10,11]. Importantly, meiotic simulations remove the geometric constraints
641 specific to the Rabl conformation[12,13] because this is not visible in meiotic pachytene *ndt80*Δ Hi-
642 C maps. As our focus was to characterize the grids of intra-chromosomal interactions, we
643 considered a system with multiple copies of chromosome 13, equivalent to four copies of the
644 haploid genome in terms of total genomic content (4 x 13 copies of chromosome 13), to enable
645 efficient computational averaging of simulated Hi-C maps. Extruded loops were generated
646 according to parameters that describe the dynamics of loop extruders, using the simulation
647 engine described in[14]: extruder *separation*, extruder *processivity*, chromatin fiber *relaxation time*
648 relative to extruder velocity, and *barrier strength*. Because yeast chromosomes are short
649 compared to higher eukaryote chromosomes, relaxation time is relatively rapid and we focused
650 on *separation, processivity,* and *barrier strength*. At every given timepoint an extruded loop is
651 realized as a bond between monomers at the two bases of the loop (see
652 ./src/examples/loopExtrusion in https://bitbucket.org/mirnylab/openmm-polymer/).
653
654 Upon encountering a barrier, a loop extruder is paused with probability according to the barrier
655 strength; barrier strength =1 indicates an impermeable barrier, barrier strength =0 indicates no

656 impediment to extrusion. We assume loop extrusion occurs independently on each chromatid,
657 and simulate loop extrusion dynamics on a 1D lattice (as in[7]) where the number of lattice sites
658 equals the total number of monomers (75,140). Bi-directional barriers were placed at monomers
659 with positions corresponding to Rec8 ChIP-seq sites[8], and pause extruders according to the
660 barrier strength parameter. We assume a uniform birth probability, constant death probability,
661 and that all barriers have an equal strength; as additional data becomes available, these
662 assumptions can be relaxed and more detailed models can be built.
663
664 We investigated scenarios where chromatids are then either left individualized (52 copies),
665 crosslinked to sisters (26 pairs), or additionally paired with homologs (13 pairs-of-pairs). For
666 simulations with sister crosslinks, these were added (following[15]) when extruded loop bases
667 were present at cognate positions ±30 monomers (~20kb) on both chromatids (distance=20nm);
668 homolog crosslinks were added similarly when sister crosslinks were present on both
669 chromatids (distance=100nm); centromeres and telomeres were always paired, and both
670 presented impermeable (strength=1) boundaries to extruders. To avoid introducing pseudo-
671 knots, if extruded loops were nested only the outer cohesins were considered as possible bases
672 for sister crosslinks, sister crosslinks were only allowed between the same side of loop bases
673 (i.e. left-to-left arm or right-to-right arm), and sister crosslinks were only added between bases
674 at the reciprocal minimum distance.
675
676 For calculation of simulated Hi-C maps, contacts were recorded from conformations of the full
677 system, which includes intra- and inter-sister, and interhomologue contacts. Because
678 experimental Hi-C here does not distinguish either sisters or homologs, contacts were then
679 aggregated into one simulated map. For each model and parameter set we investigated, we
680 collected an ensemble of conformations, generated simulated chr13 Hi-C maps, and compared
681 their features and *P(s)* with those from experimental Hi-C maps. Each simulated chr13 map
682 represented an average over 5400 conformations. *P(s)* for chr13 was calculated from 2kb
683 binned simulated maps exactly as for experimental maps. Maps of goodness-of-fit between
684 simulations and experimental data (e.g. **Fig. 3b,c**) were computed as the geometric standard
685 deviation of the ratio of simulated to experimental *P(s)* combined across $P^{Rec8\text{-}Rec8}(s)$, $P^{Rec8\text{-}non}(s)$,
686 and $P^{non\text{-}non}(s)$, as was previously done for P(s) within TADs of multiple sizes and between
687 TADs[7], for *s* from 10kb to 300kb. This measure reflects the typical fold-deviation for *P(s)*.
688
689 Simulated ChIP-seq profiles (**Extended Data Fig. 6b**) for Rec8 were generated by aggregating
690 the position of extruded loop bases (two per extruded loop) across conformations. Statistics of
691 extruded loop positioning relative to Rec8 sites was calculated with *loopstats.py* in *looplib*

692 (https://github.com/golobor/looplib), and arc diagrams (**Extended Data Fig. 6c**) with *loopviz.py*.
693 Conformations showing chromatids or positions of extruded loop bases were rendered in
694 PyMOL (https://pymol.org/sites/default/files/pymol.bib).
695
696
697

698 References (Methods)

699

700 1. Belton, J. M. & Dekker, J. Hi-C in Budding Yeast. *Cold Spring Harb Protoc* **2015**, 649-661
701 (2015).
702 2. Servant, N. et al. HiC-Pro: an optimized and flexible pipeline for Hi-C data processing.
703 *Genome Biol* **16**, 259 (2015).
704 3. Hsieh, T. S., Fudenberg, G., Goloborodko, A. & Rando, O. J. Micro-C XL: assaying
705 chromosome conformation from the nucleosome to the entire genome. *Nat Methods* **13**,
706 1009-1011 (2016).
707 4. Mizuguchi, T. et al. Cohesin-dependent globules and heterochromatin shape 3D genome
708 architecture in S. pombe. *Nature* **516**, 432-435 (2014).
709 5. Crane, E. et al. Condensin-driven remodelling of X chromosome topology during dosage
710 compensation. *Nature* **523**, 240-244 (2015).
711 6. Nora, E. P. et al. Targeted Degradation of CTCF Decouples Local Insulation of
712 Chromosome Domains from Genomic Compartmentalization. *Cell* **169**, 930-944.e22
713 (2017).
714 7. Fudenberg, G. et al. Formation of Chromosomal Domains by Loop Extrusion. *Cell Rep*
715 **15**, 2038-2049 (2016).
716 8. Ito, M. et al. Meiotic recombination cold spots in chromosomal cohesion sites. *Genes Cells*
717 **19**, 359-373 (2014).
718 9. Schalbetter, S. A. et al. SMC complexes differentially compact mitotic chromosomes
719 according to genomic context. *Nat Cell Biol* **19**, 1071-1080 (2017).
720 10. Eastman, P. et al. OpenMM 7: Rapid development of high performance algorithms for
721 molecular dynamics. *PLoS Comput Biol* **13**, e1005659 (2017).
722 11. Eastman, P. & Pande, V. S. Efficient nonbonded interactions for molecular dynamics on
723 a graphics processing unit. *J Comput Chem* **31**, 1268-1272 (2010).
724 12. Wong, H. et al. A predictive computational model of the dynamic 3D interphase yeast
725 nucleus. *Curr Biol* **22**, 1881-1890 (2012).
726 13. Tjong, H., Gong, K., Chen, L. & Alber, F. Physical tethering and volume exclusion
727 determine higher-order genome organization in budding yeast. *Genome Res* **22**, 1295-
728 1305 (2012).
729 14. Fudenberg, G. & Imakaev, M. FISH-ing for captured contacts: towards reconciling FISH
730 and 3C. *Nat Methods* **14**, 673-678 (2017).
731 15. Goloborodko, A., Imakaev, M. V., Marko, J. F. & Mirny, L. Compaction and segregation of
732 sister chromatids via active loop extrusion. *Elife* **5**, (2016).

733

Figure 1

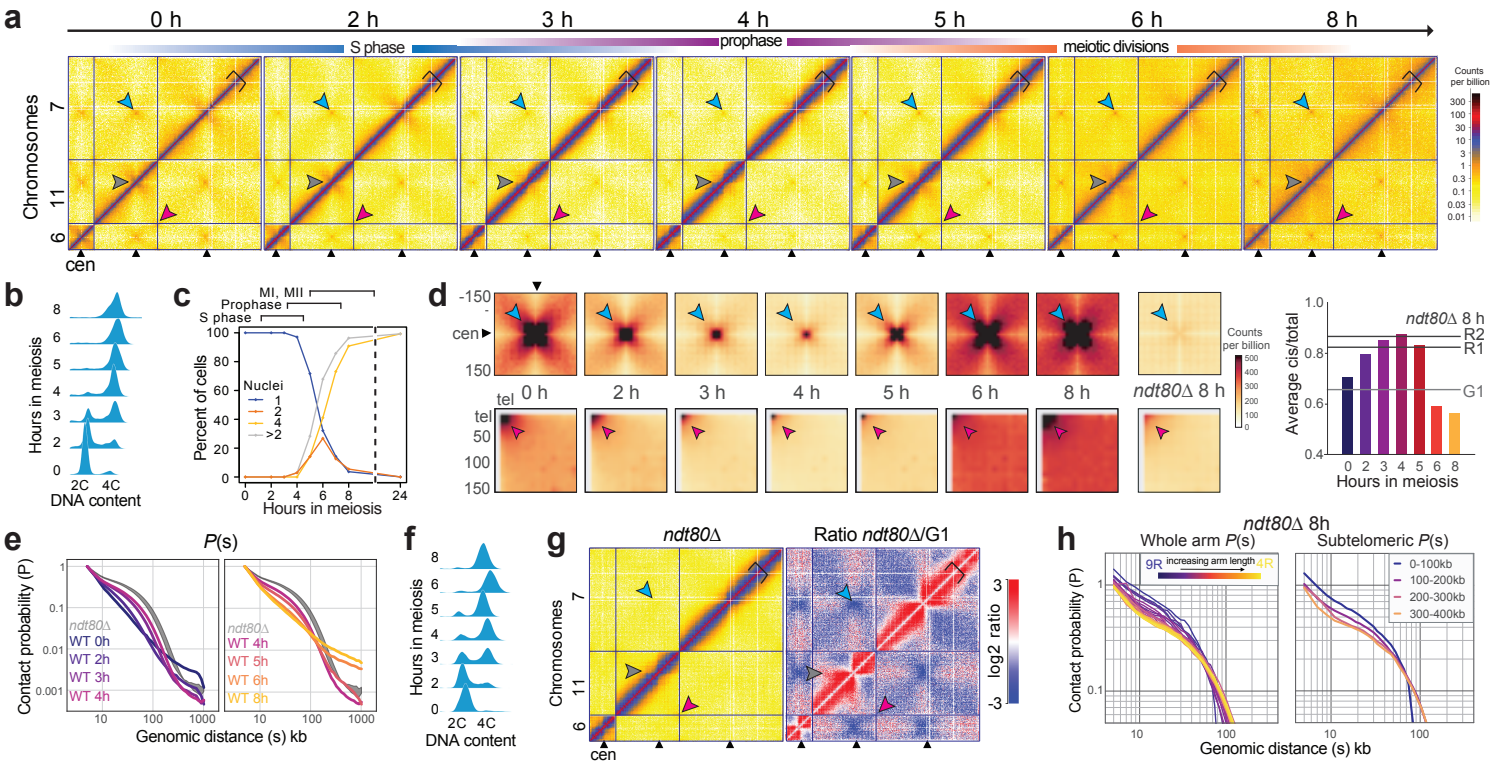

Figure 1. Chromosome conformation during yeast meiosis.
a. Cells were collected during meiosis at indicated timepoints and analysed by Hi-C. At 0h the cells are in G1. Representative Hi-C contact maps of chromosomes 6, 11, and 7 plotted at 5 kb resolution. Centromeres, telomeres and arm fold-back at the centromere are indicated by blue, red and grey arrows, respectively, and axial compaction by the width of the main diagonal relative to the fixed-width black clamp. For interactive HiGlass[52] views see: http://higlass.pollard.gladstone.org/app/?config=Z5iwKpjzQpePCXXyvuYGeQ
b. Meiotic entry assessed by FACS; at 4 h, the majority of cells show a 4C peak indicating completion of DNA replication.
c. Meiotic progression was monitored by quantification of nuclear divisions determined by DAPI staining. Around 4 h, cells start to undergo meiotic divisions I and II. The majority of cells undergo meiotic divisions between 4 and 8 h, indicating the degree of heterogeneity within the cell population.
d. *Upper panels*: Average *trans* centromere-centromere contact maps. *Lower panels*: *trans* telomere-telomere contact maps. *Right*: ratio of *cis* to total contact frequency.
e. Intra-arm contact probability versus genomic distance, *P(s),* indicating the emergence (*left*) and disappearance (*right*) of chromosome arm compaction during meiosis. Shaded area bounded above and below by the two *ndt80*Δ 8h replicates.
f. Meiosis was induced in *ndt80*Δ cells for 8h and meiotic entry was checked by monitoring DNA replication by FACS.
g. *ndt80*Δ cells were grown for 8h in sporulation media and analysed by Hi-C (*left*). Log2 ratio of *ndt80*Δ cells 8h over G1 (*right*). Centromeres and telomeres are indicated by blue and red arrows, respectively, and axial compaction by a black clamp.
h. *Left*: Contact probability of individual chromosome arms stratified by length. *Right*: Contact probability stratified by the distance from the telomere.

Figure 2

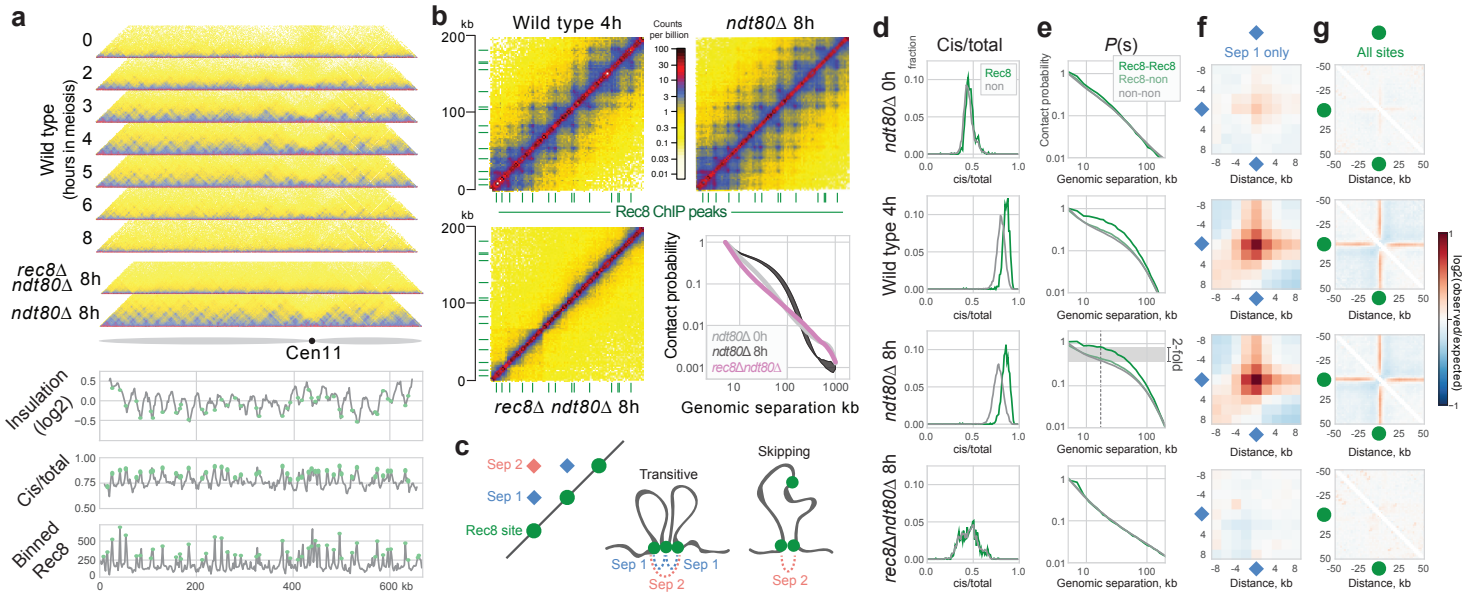

Figure 2. Emergence of a Rec8-dependent grid of punctate interactions in meiosis

a. Hi-C contact maps of chromosome 11 for the indicated genotypes plotted at 2 kb bin resolution, showing near-diagonal interactions. Wild type timepoints as in **Fig. 1a**. **Lower panels**: log2(insulation); cis/total ratio, Rec8 ChIP-seq[28], all binned at 2kb. Insulation and cis/total calculated from *ndt80*Δ maps. Positions of Rec8 sites indicated as green circles. Genome-wide cis/total (Spearman's R=0.62, P<1e-10) and insulation (R= -0.23, P<1e-10, insulation window = 20 kb) profiles are correlated with Rec8 occupancy.

b. Zoom-in into contact maps on chromosome 11 (0-200kb) of wt-4h and *ndt80*Δ (top) and *rec8*Δ (*bottom left*). Contact probability versus genomic distance, *P(s)*, for G1(*ndt80Δ-0h*) and *ndt80*Δ and *rec8*Δ (*bottom right*). Data shown is the average (n=2) except for wt-4h. Rec8 peak sites called from ChIP-seq data[28] are indicated in green. For an interactiveview see: http://higlass.pollard.gladstone.org/app/?config=Twrh61jGT4SlxotaguTIJg

c. Simplified illustration of how a grid of peaks on a Hi-C map can emerge between Rec8 sites either by transitive contacts between adjacent loops, or by loops that skip over adjacent sites. Experimentally observed grids extend much further than separation=2 (**Extended Data Fig. 4c**)

d. Cis/total ratios for Rec8 (green) and nonRec8 (grey) sites for indicated datasets.

e. Contact frequency versus distance between Rec8-Rec8 sites (green), Rec8-nonRec8 sites (light green) and nonRec8-nonRec8 sites (green).

f. Log2 ratio of contact frequency between adjacent Rec8-sites (separation=1) compared to average cis interactions.

g. Log2 ratio of contact frequency centered at Rec8 sites compared to average cis interactions.

In *ndt80*Δ, Rec8 sites show: elevated cis/total frequency (0.85 versus 0.77), elevated pairwise contact frequency (~2-fold at 20 kb), and mild insulation. These distinctions are similar in wild type pachytene (4h) yet absent in G1 (*ndt80Δ-0h*) or in *rec8*Δ.

Figure 3

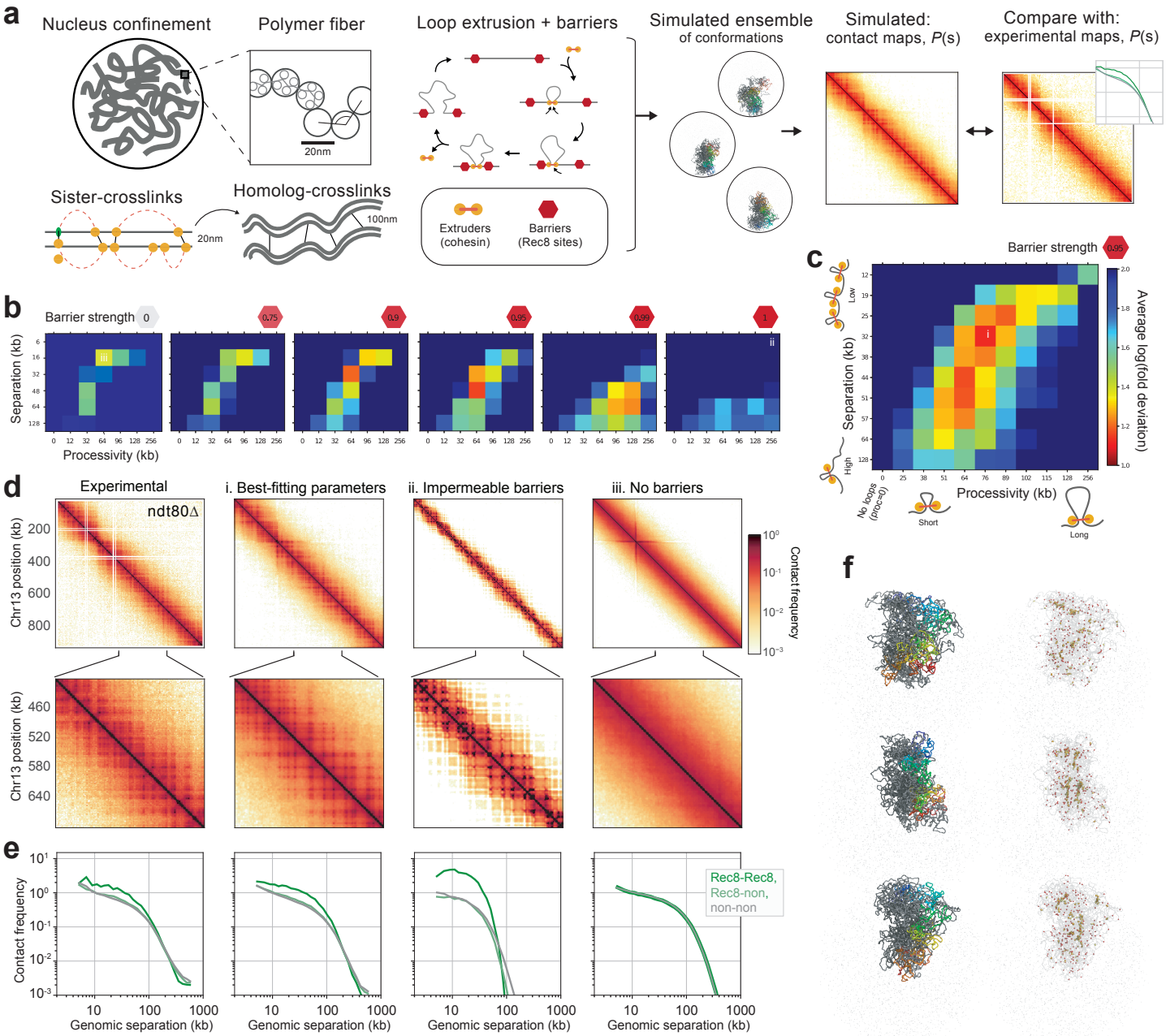

Figure 3. Model for meiotic chromosome compaction in prophase.

a. In simulations, yeast chr13 was represented as a polymer fiber confined to the nucleus subject to additional meiosis-specific constraints. These include: extruded loops, sister crosslinks, and homolog crosslinks (**Methods**). Barriers to extruded loops were placed at Rec8 sites[28]. We imposed inter-sister and inter-homologue crosslinks at sites of extruded loop bases in order to approximate the paired arrangement of homologues at pachytene (**Extended Data Fig. 6**). For each set of extruded loop parameters (*processivity, separation,* and *barrier strength*), conformations were collected and used to generate simulated contact maps. These were then compared with experimental contact maps via the combined average fold discrepancy with *P(s)* curves for Rec8-Rec8, Rec8-non, and non-non bin pairs at 2 kb resolution.

b. Goodness-of-fit for indicated barrier strengths over coarse grids of processivity and separation demonstrate that intermediate barrier strengths are required to agree with experimental *ndt80*Δ Hi-C maps.

c. Goodness-of-fit for a fine grid of processivity versus separation at barrier strength 0.95. Best-fitting models had separation ~32kb and processivity ~76kb, corresponding to ~60% coverage of the genome by extruded loops of average length 26kb.

d. From *left* to *right*: contact maps for chr13 for *ndt80Δ*, and simulations with (i) best-fitting parameters, (ii) relatively stable loops between neighboring Rec8 sites, and (iii) no barriers.

e. P(s) split by Rec8-Rec8, Rec8-non, and non-non, as in **Fig. 2d**.

f. Conformations for best-fitting simulations, which highlight: (*left)* one chromatid colored from start (red) to end (blue); *(right*) extruders (yellow), extrusion barriers (red), and extruders paused at barriers (orange).

Figure 4

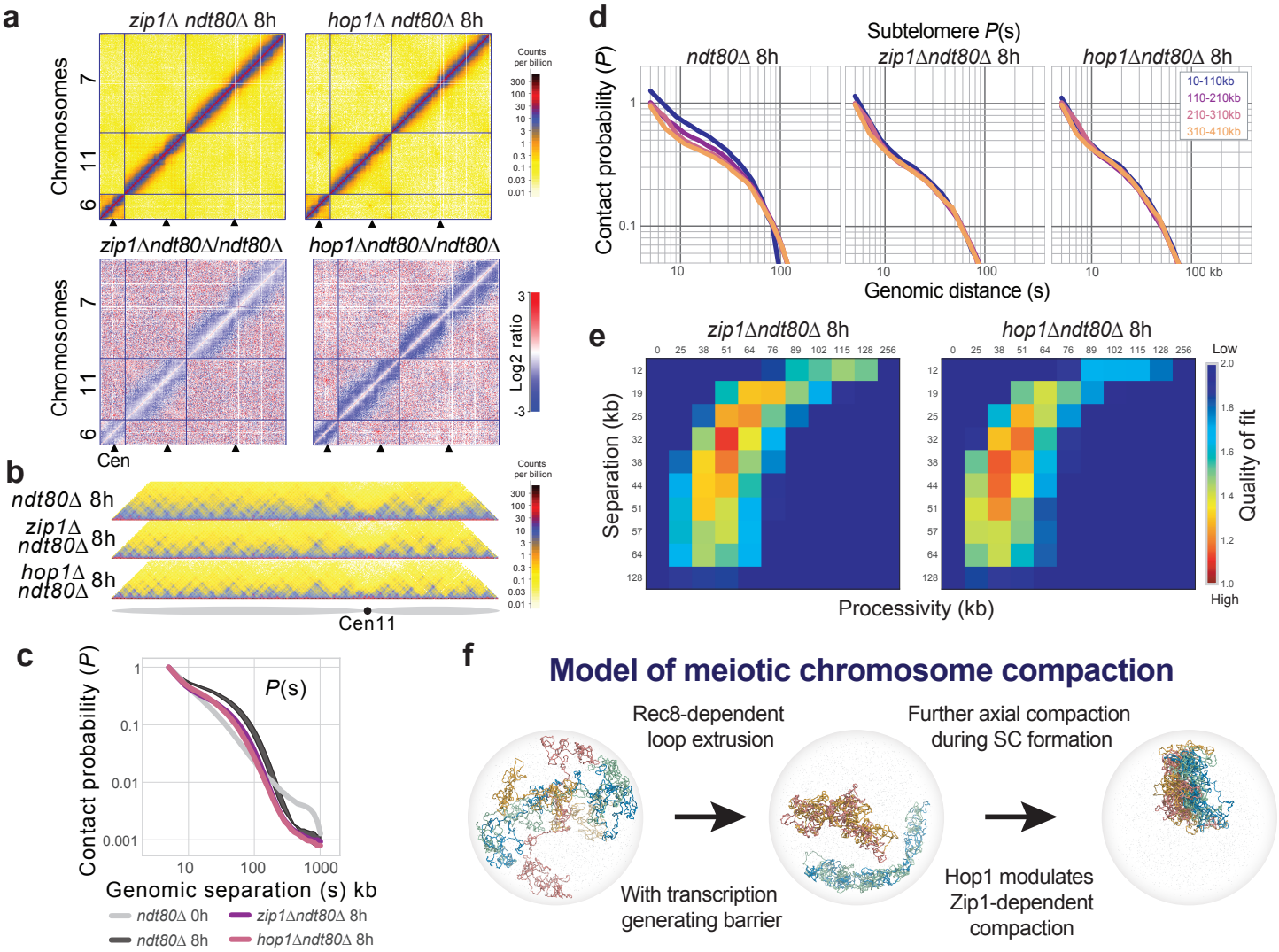

Figure 4. Hop1 and Zip1-dependent compaction of Rec8-dependent loops.
a. *Top*: Hi-C maps for *hop1*Δ and *zip1*Δ (plotted as in **Fig. 1a**). *Bottom*: Log2 ratio of hop1Δ over *ndt80*Δ (as in **Fig. 1g**). For interactive views of the full genome, see http://higlass.pollard.gladstone.org/app/?config=TTBGu5DDR0SHAa09zrjTXA
b. Hi-C contact maps of chromosome 11 for *hop1*Δ and *zip1*Δ plotted at 2kb bin resolution, showing near-diagonal interactions, as in **Fig. 2a**.
c. Contact probability versus genomic distance for G1, *ndt80*Δ, *hop1*Δ, *zip1*Δ. Shaded area bounded above and below by *ndt80*Δ replicas. Average between two replicas for *zip1*Δ and one sample for G1 and *hop1*Δ are shown.
d. Contact probability over genomic distance averaged over all chromosome arms stratified by distance from the telomere.
e. Goodness-of-fit for simulations without homolog crosslinks with a fine grid of processivity versus separation at barrier strength 0.95 *zip1*Δ and *hop1*Δ.
f. Model of meiotic chromosome compaction: Rec8-dependent loop formation leads to initial chromosome arm compaction and emergence of a grid-like pattern of Hi-C interactions that jointly agrees with a mechanism of loop extrusion including barrier elements. We suggest that transcription could impose such barriers. Hop1 and Zip1 are dispensable for this step, but are required for synapsis, where additional compaction occurs differentially along chromosome arms.

Extended Data Figure 1

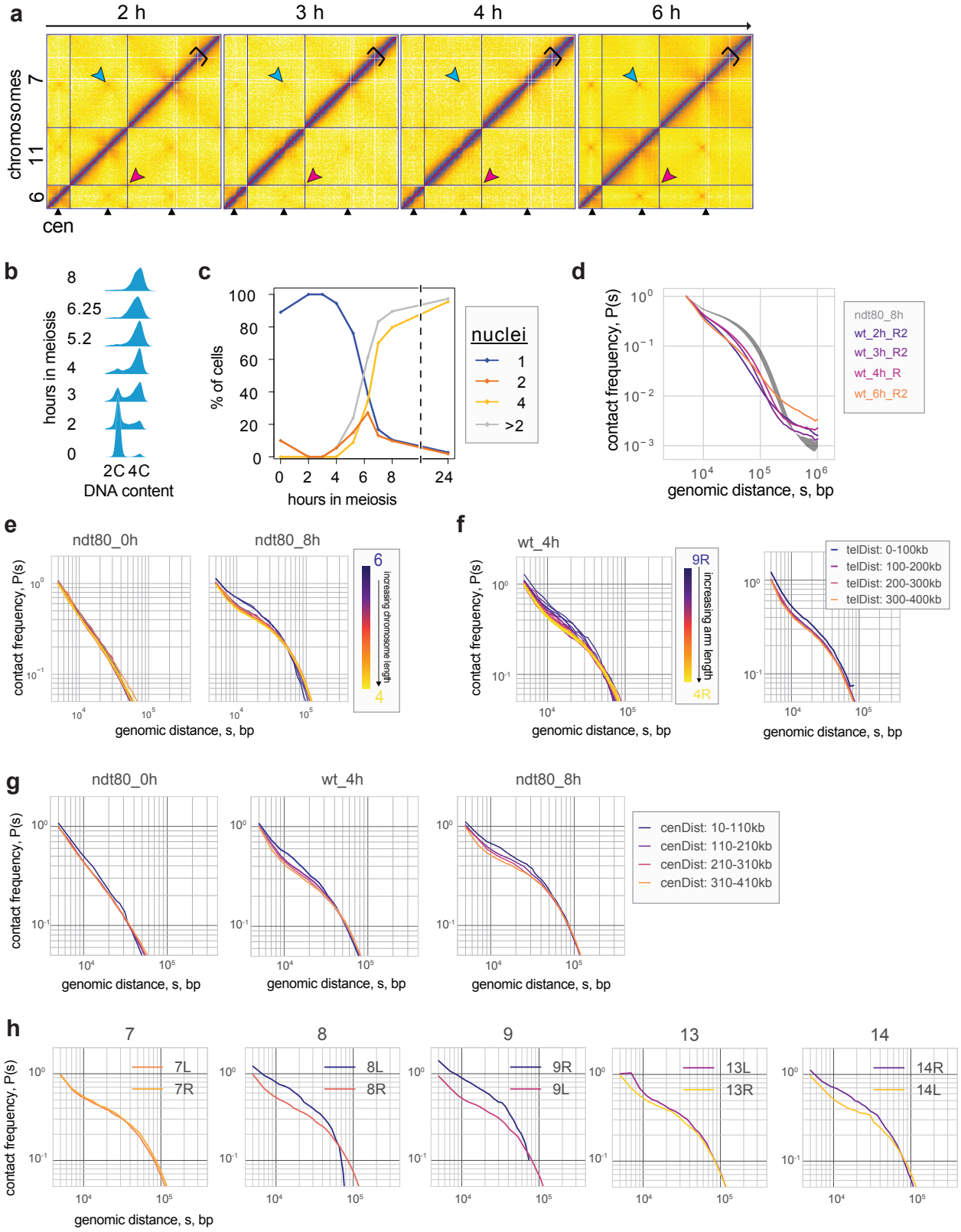

Extended Data Fig. 1
a-d. Results from a replicate timecourse, collected and characterized independently of the timecourse in Fig. 1.
a. Hi-C maps, plotted as in Fig. 1a.
b. FACS as in Fig. 1b.
c. DAPI as in Fig. 1c.
d. *P(s)* as in Fig. 1e.
e. *P(s)* for chromosomes stratified by size for *ndt80*Δ-0h, *ndt80*Δ-8h. Short chromosomes display relatively elevated *P(s)* at short distances, and an earlier shoulder.
f. *Left*: *P(s)* for individual chromosome arms, stratified by size for wt-4h. Short arms display relatively elevated *P(s)* at short distances, and an earlier roll-over. *Right*: Intra-arm *P(s)* stratified by the distance from the telomere for wt-4h, averaged across all chromosomes. Telomere-proximal regions display elevated *P(s)* at short distances.
g. Intra-arm *P(s)* stratified by the distance from the centromere for G1 (*ndt80*Δ-0h), *wt*-4h, *ndt80*Δ-8h, averaged across all chromosomes.
h. Contact probability of single chromosome arms for *ndt80*Δ-8h.

Extended Data Figure 2

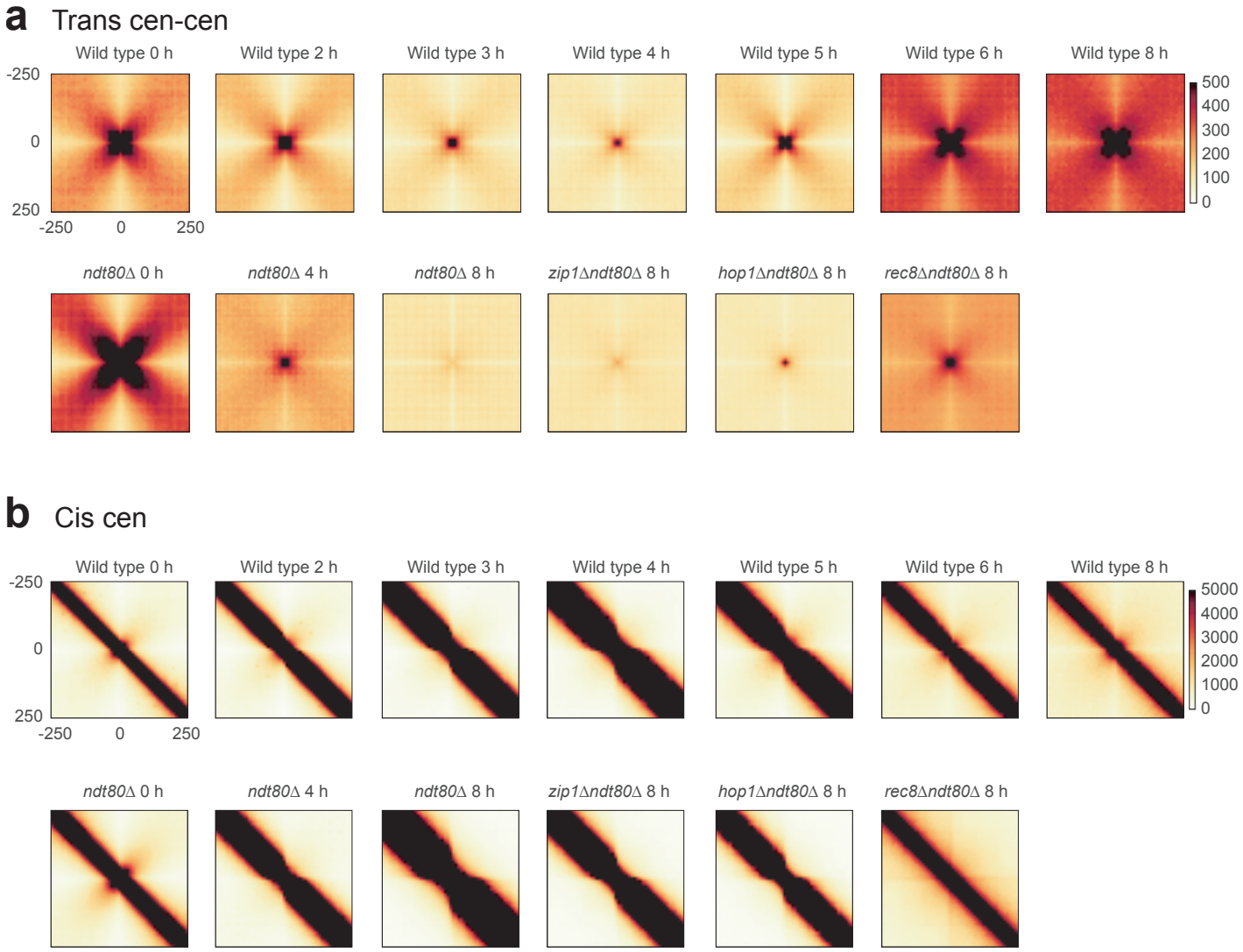

Extended Data Fig. 2
a. Average *trans* centromere-centromere contact maps for indicated data sets.
b. Average *cis* centromere-centromere contact maps for indicated data sets. Note the loss of the folding back in meiosis, and how the intra-arm enrichment is insulated at centromeres in meiosis.

Extended Data Figure 3

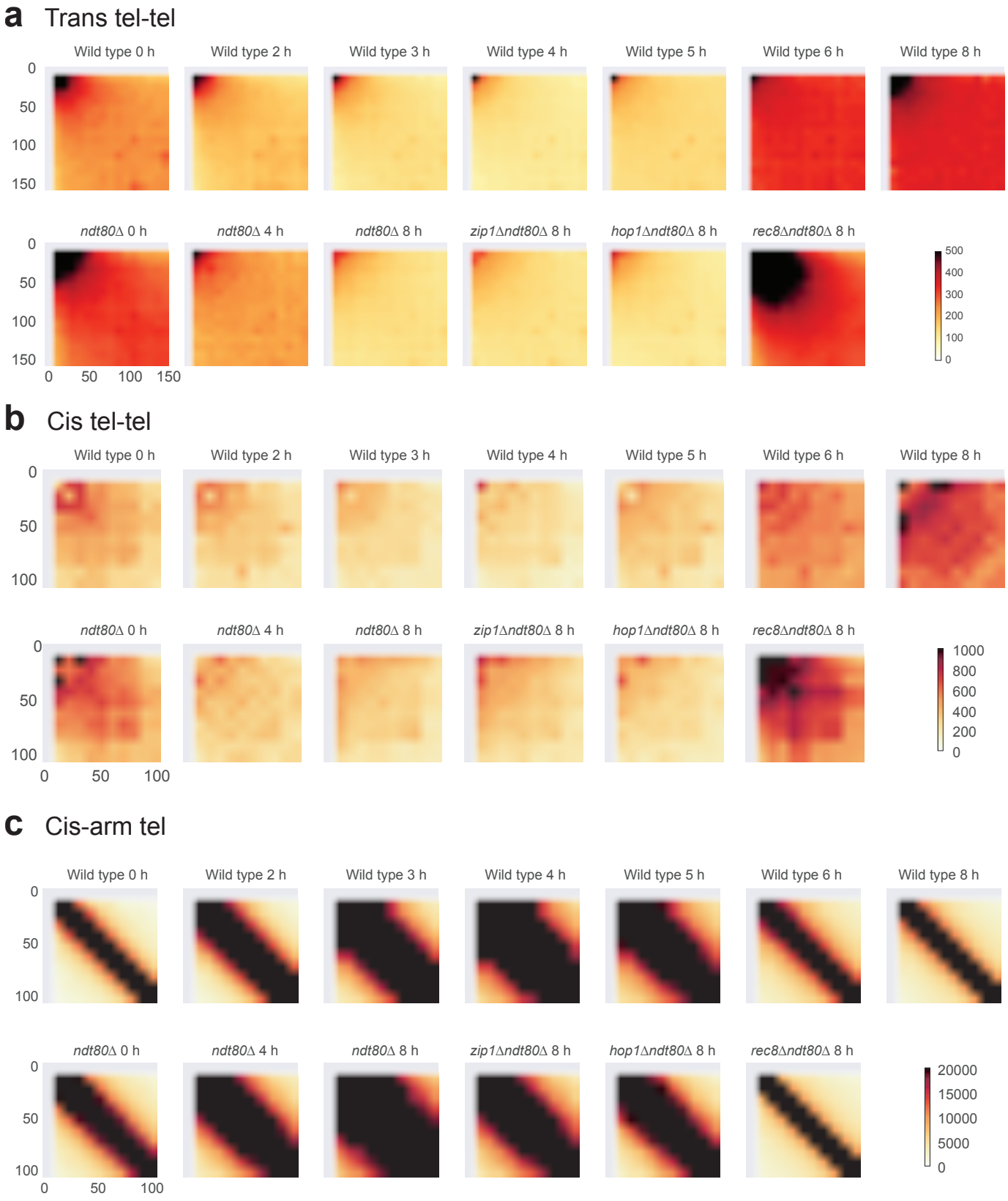

Extended Data Fig. 3
a. Average *trans* telomere-telomere contact maps for indicated datasets.
b. Average telomere-telomere contact maps between the two telomeres of the same chromosome.
c. Average contact map around each telomere in *cis.*

Extended Data Figure 4

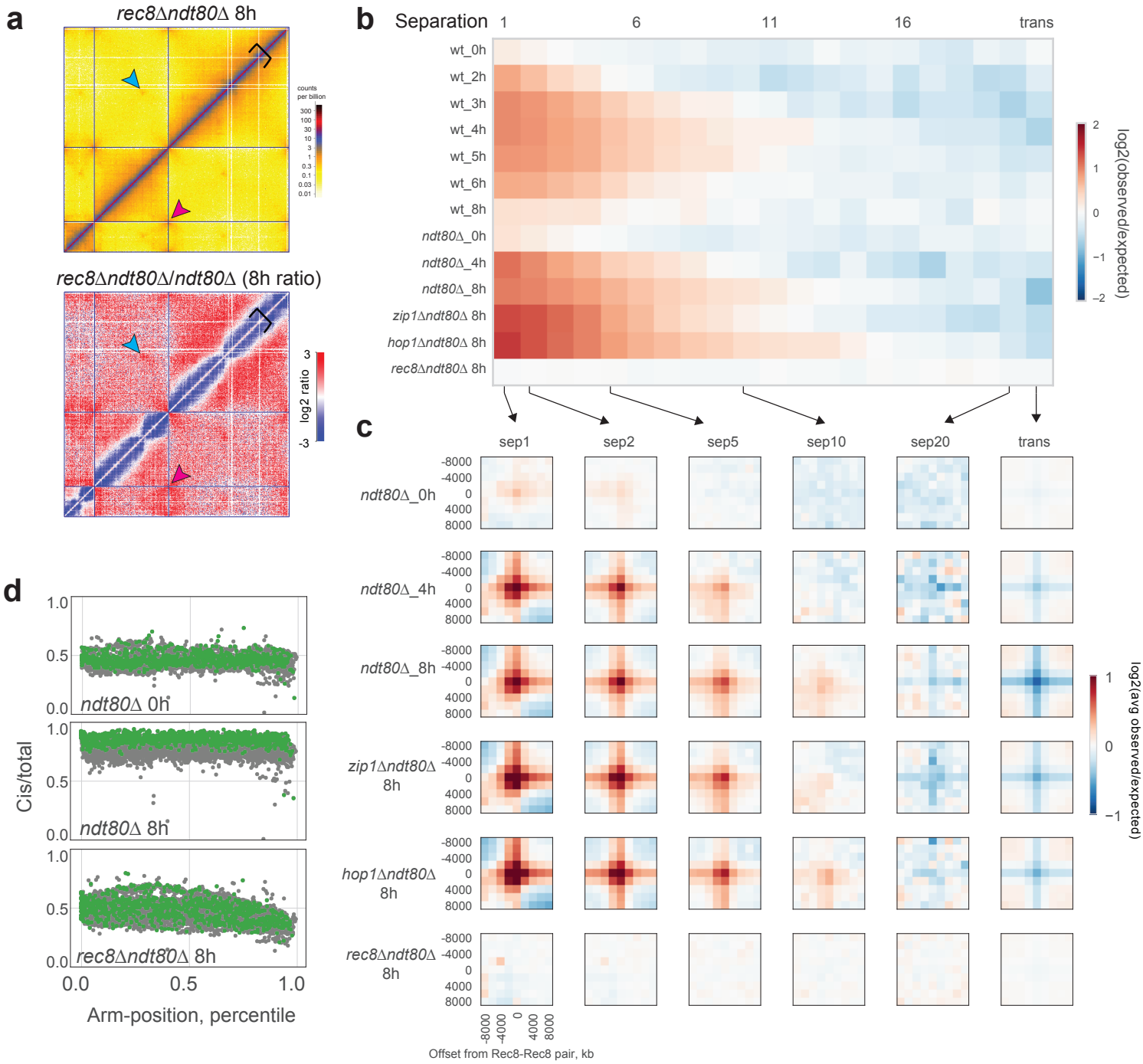

Extended Data Fig. 4

a. *Left*: Hi-C contact maps of *rec8Δ ndt80Δ*. Chromosomes 6, 11 and 7 are shown as representatives for the whole genome. *Right*: Log2 Hi-C ratio maps of *rec8Δ ndt80Δ* / *ndt80Δ*. Plotted as in Fig. 1g.

b. Log2 observed over expected contact frequency at Rec8-Rec8 peak pairs as a function of separation across datasets.

c. Log2 observed over expected contact frequency +/-8 kb around Rec8-Rec8 peak pairs at the indicated separations. Together, **b-c** demonstrate that Rec8-Rec8 enrichments are strongest between adjacent sites, decrease between non-adjacent sites with increasing genomic separation, and are absent in *trans*. Equally important, these meiotic features are lost in *rec8Δ*. As for mammalian interphase, this observation in meiosis argues for a *cis*-acting process underlying the formation of focal interactions between Rec8 sites.

d. cis/total as a function of distance along the chromosomal arm, Rec8 sites marked in green.

Extended Data Figure 5

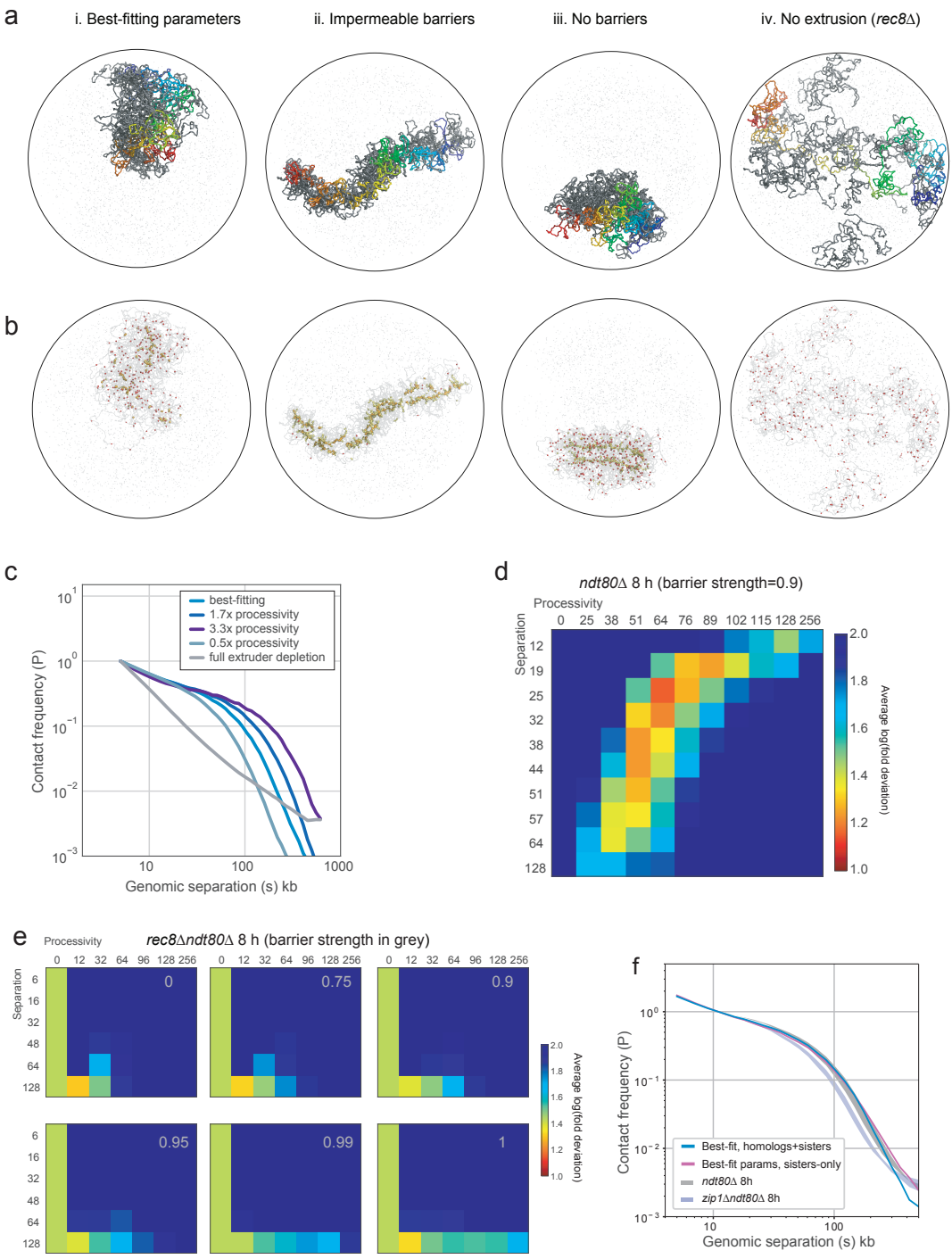

Extended Data Fig. 5

a. Representative conformation for the indicated parameter sets. As in **Fig. 3F,** one chromatid from a homologous quartet of chromatids coloured from start to end according to the spectrum; other three coloured in grey.

b. For the same three conformations, positions of Rec8 sites indicated with red spheres, positions of extruded loop bases in yellow, and extruders overlapping a Rec8 site in orange. Note the stable loops between neighbouring Rec8 sites creates a very elongated chromatid (ii). Also note the majority of Rec8 sites are unoccupied in (iii), despite the self-assembly of two axial cores and a strong brush. Finally, note very dispersed chromosomes in (iv), consistent with EM[3] for *rec8Δ*.

c. Contact frequency versus distance, *P(s),* for indicated simulations. Note that the loss of the shoulder in *P(s)* in the case of full extruder depletion mirrors the difference between experimental *ndt80Δ* and *rec8Δ* Hi-C maps. Simulations with increased processivity predict that *P(s)* would shift rightward if unloading was impaired, as could happen in *waplΔ*. Conversely, if unloading was enhanced, simulations with decreased processivity indicate a leftward shift in P(s), until the absence of extruders.

d. Goodness-of-fit for a fine grid of processivity versus separation at barrier strength 0.90. The best-fit occurs at similar processivity and separation as for barrier strength 0.95 shown in **Fig. 3c**, but with slightly lower goodness-of-fit.

e. Goodness-of-fit to *rec8Δ* data for simulations with the indicated barrier strengths (in grey: 0.00, 0.75, 0.90, 0.95, 0.99, 1.00) over coarse grids of processivity and separation demonstrates that the best fits have few if any extruded loops, regardless of barrier strength.

f. *P(s)* curves for simulations with sisters and homologs with the best-fitting parameters for *ndt80Δ-8h* maps compared to P(s) for simulations with sisters only show that simply removing homolog tethering does not recapitulate the sort of shifted P(s) seen experimentally in *zip1Δ* Hi-C.

Extended Data Figure 6

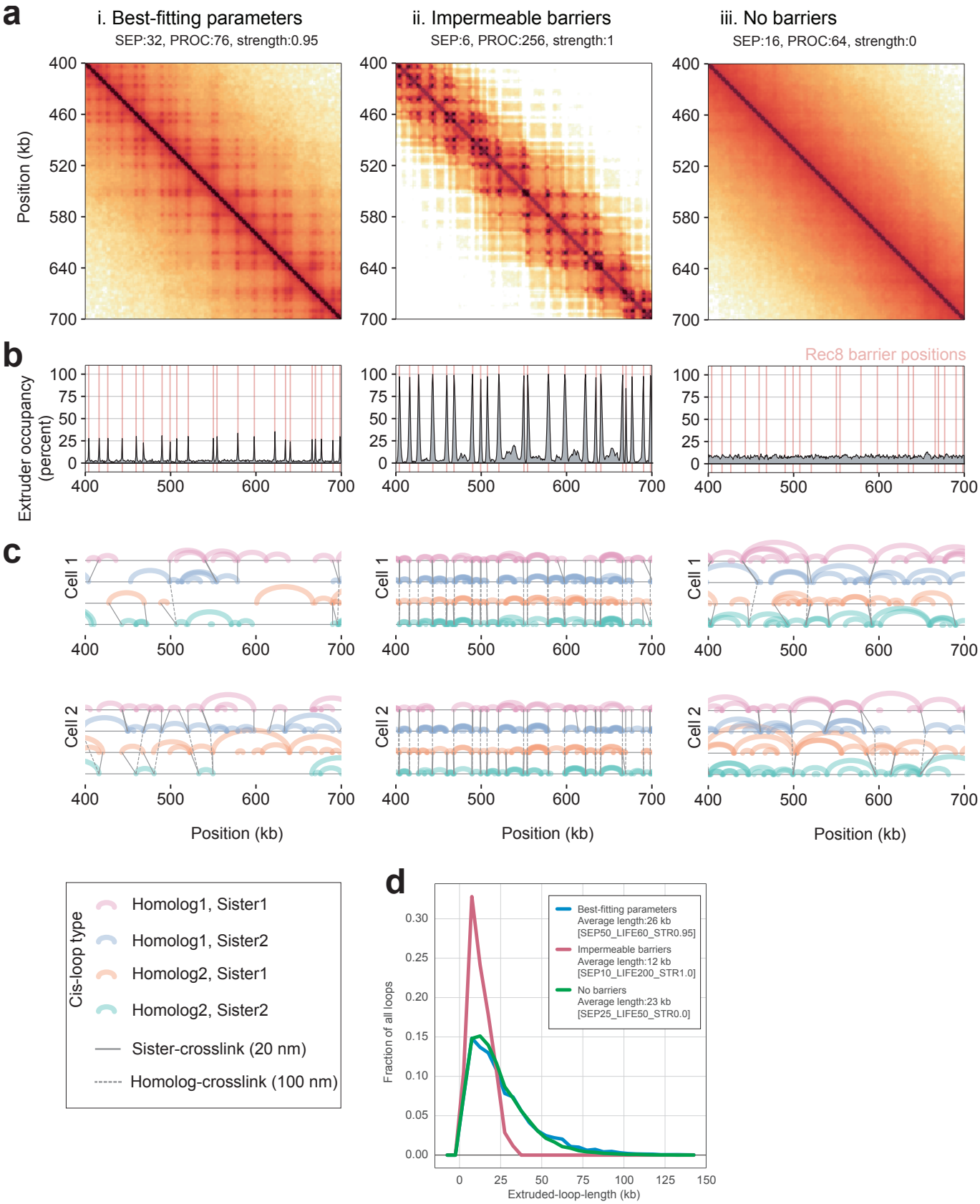

Extended Data Fig. 6

a. Simulated contact maps for the indicated region of chr13 for: (i) best-fitting simulations, (ii) simulations with relatively stable loops between neighboring Rec8 sites (barrier strength=1 and high processivity), and (iii) no barriers, as in **Fig. 2d.**

b. Simulated ChIP-seq profiles for the indicated region of chr13. Best-fitting simulations (i) display occupancy well below 100% at Rec8 sites. Simulations with stable loops (ii) display highly occupied Rec8 sites. Simulations without barriers (iii) have homogenous Rec8 occupancy across the genome.

c. Positions of extruded loops (arcs) sister crosslinks (solid black lines) and homolog crosslinks (dashed lines) for four chromatids in two separate cells, showing how the simulated Hi-C maps and ChIP-seq profiles emerge from the stochastic positioning of extruded loops from cell-to-cell. For statistics, see **Supplementary Table S1**.

d. Histogram of extruded loop lengths for indicated parameters (i, ii, iii).